Thermal conductivity of ^{4}He I from near T_λ to 3.6 K and vapor pressure to 30 bars

W. Y. Tam and Guenter Ahlers
Department of Physics, University of California, Santa Barbara, California 93106
(Received 11 June 1985)

We present new data for the thermal conductivity of liquid ^{4}He along isotherms from 2.1 to 3.6 K, covering the pressure range from vapor pressure to 30 bars, and along isobars from vapor pressure to 28 bars, covering the reduced-temperature range $2\times10^{-6}\lesssim t\,[=(T-T_\lambda)/T_\lambda]\lesssim0.1$. Measurements in several cells with spacings from 0.0025 to 0.453 cm revealed no anomalous size effect. For $t\gtrsim10^{-3}$, the accuracy of the data is 0.2% to 0.3%. Closer to T_λ systematic errors due to uncertainties in boundary-resistance corrections gradually increase with decreasing t, and reach about 2% near $t=2\times10^{-6}$. With decreasing $t\lesssim10^{-4}$ random errors due to finite temperature resolution increase also, and reach about 2% near $t=2\times10^{-6}$.

I. INTRODUCTION

The dynamics of the superfluid transition of ^{4}He has provided us with a highly quantitative testing ground of the predictions of the renormalization-group theory (RGT) of critical phenomena.[1] The primary reasons for this are of both theoretical and experimental origin. On the one hand, highly quantitative measurements are possible for this system over a wide range of the reduced temperature $t=T/T_\lambda-1$ and the pressure P.[2] On the other hand, quantitative theoretical predictions[3] are possible because there exists a wide range of t, roughly $t\gtrsim10^{-3}$ or 10^{-4}, where the dynamic coupling constant of the RGT model[4] for this transition is a small parameter and the perturbation expansion of the theory is a controlled approximation.[5] For smaller t, the coupling constant of the theory becomes of order unity, and the existence of a weak- to strong-coupling crossover at temperatures accessible to quantitative experimental measurements enhances the interest in this particular transition.

The most quantitative comparison of experiment with theoretical predictions that can be made at the present time pertains to the thermal conductivity λ above the transition temperature T_λ. The best opportunity for a quantitative comparison exists at the higher pressures where the weak-coupling regime extends to the smallest values of t.[5] For P greater than the saturated vapor pressure (SVP), there is a great scarcity of experimental data near $T_\lambda(P)$. The pioneering work of Kerrisk and Keller[6] had indeed revealed the existence of a strong singularity in λ near $T_\lambda(P)$, but the data gave little information about its quantitative nature. At vapor pressure, more quantitative data with higher temperature-resolution soon became available over a wide range,[7–10] but the early data at higher pressures[10] were unfortunately restricted to the range $t\lesssim3\times10^{-4}$. The early experimental work at small t was also subject to systematic errors associated with uncertainties in the contribution of the walls to the heat conduction,[9,10] of the boundary resistance to the total thermal resistance,[9,10] and of an unexplained and surprisingly large size effect[7,8] encountered in cells of small spacing. In the present paper we present new experimental results for λ which cover a wide range of t and P and are not subject to large systematic errors from wall conduction and boundary-resistance corrections. They also do not show the size effect reported previously.[7,8] In a subsequent paper[11] we plan to compare these data with the predictions[3] of the renormalization-group theory.[4]

Our measurements were made along various isotherms from 2.1 to 3.6 K covering the pressure range from SVP to 30 bars, and along isobars from SVP to 28 bars covering the reduced-temperature range from 2×10^{-6} to 10^{-1}. We used cells with spacings d which ranged from 0.0025 to 0.453 cm. Only for cells with $d\gtrsim0.1$ cm could the spacing be measured with an absolute accuracy of a fraction of 1%. Therefore, absolute measurements of high accuracy are restricted to the larger cell sizes. The largest cell, however, had rather long thermal relaxation times, and, therefore, the data obtained from it did not have the highest precision. Our most accurate and precise data were obtained in cell F which had a spacing of 0.203 cm. For that cell, the isotherm data have an accuracy of 0.2% to 0.3%. They agree with the measurements by Kerrisk and Keller[6] within the uncertainty of the earlier work of 1% to 2%. At SVP the cell-F data agree well with other absolute measurements by Dingus *et al.*,[12] by Steinberg and Ahlers (cell *G*),[13] and by Ahlers and Behringer (cell A).[14]

The cell-F data span the pressure range from 0 to 28 bars and at each pressure the reduced-temperature range from 2×10^{-6} to 1. At all pressures they are systematically lower at small t than the older "cell D" data[10] (which only exist at small t). We attribute this difference to the systematic errors in the older measurements which we mentioned above (see also Sec. II A of Ref. 5).

For the present measurements we essentially eliminated systematic errors associated with the wall conduction by estimating the heat carried by the walls from numerical solutions of the two-dimensional heat-flow problem involving the copper top and bottom plates, the walls, and the fluid. We attempted to deal with the problem caused by the boundary resistance R_b by measuring R_b in the superfluid phase and by using cells of several thicknesses. For $t\gtrsim10^{-3}$, any uncertainty in λ due to R_b is quite

negligible for cell F. However, at small t, even our best data are subject to small systematic errors from this source. Thus, we estimate that possible systematic errors in λ for cell F may be 0.6% at $t=10^{-4}$, 1.0% at $t=10^{-5}$, and 2% at $t=2\times10^{-6}$.

We made measurements also in a cell with the extremely small spacing $d=0.0025$ cm (cell I). These data are not very accurate because boundary-resistance corrections are large and because the large heat currents which are required do not lend themselves to very accurate measurements. However, the results agree quite well with our cell F data and do not reveal a size effect of the magnitude observed by others.[7,8]

The remainder of this paper is organized as follows. In Sec. II we describe the experimental apparatus, the procedures, and the data analysis. The results are given in Sec. III. They are discussed separately for isotherms (Sec. III B) and isobars (Sec. III C). The isobar data at small t are expressed in terms of the effective amplitude $\hat{R}_\lambda$ of λ. The effect of changing the boundary resistance is explored in detail in this section. Section IV provides a summary of our work. A number of appendixes deal with the details of the wall-conduction corrections, the boundary resistance, curvature corrections, cell-spacing determinations, and with the derivation of the specific heat at constant pressure (which is needed to calculate $\hat{R}_\lambda$ from λ) from existing thermodynamic data.

II. EXPERIMENT

A. Cryogenic apparatus

Figure 1 shows a schematic diagram of the cryogenic apparatus. This apparatus is similar to some of those used previously[15–17] for the study of ^{4}He near the λ point. The entire assembly was contained in a stainless-steel vacuum can immersed in a liquid-helium bath which could be kept at 4.2 K or pumped to a lower temperature as needed.

The top level inside the can was a continuously operating ^{4}He refrigerator[18] with a volume of about 15 cm^3. It was filled from the bath through a sintered copper filter and a supply line consisting of a 0.025-cm-i.d. stainless-steel capillary of length 30 cm into which a stainless-steel wire of 0.024 cm o.d. and of length 30 cm had been inserted. The refrigerator operated at about 1.4 K. Its temperature was stable to a few mK, and its cooling power was about 20 mW.

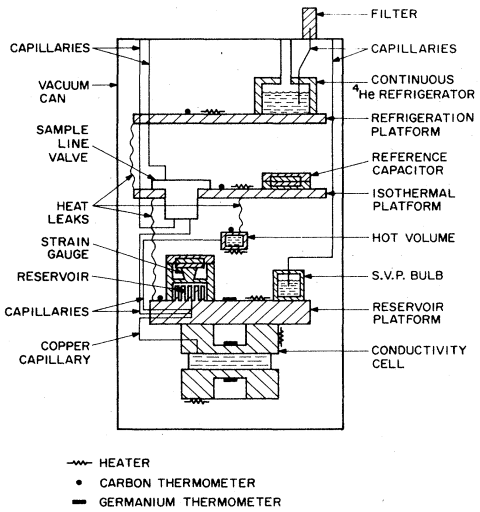

FIG. 1. Schematic diagram of the cryogenic apparatus.

Below the refrigerator was an isothermal platform[19] which was regulated at a temperature between 1.6 and 2.0 K with a stability of a few μK. It provided a stable thermal environment for the sample. Mounted on this stage was the hydraulically operated sample-line valve[20] and the pressure-gauge reference capacitor. A small volume, known as the "hot volume,"[15] of about 1 cm^3 was attached to this stage through a thin-walled stainless-steel tube which had a heat conductance of approximately 4×10^{-5} W/K. The hot volume served to control the pressure of the experimental cell as discussed in Ref. 15.

Below the isothermal platform was the reservoir platform (see also Fig. 2). It was made of thick oxygen-free high-conductivity (OFHC) copper and was structurally supported from the isothermal platform by three thin-walled stainless-steel tubes whose thermal conductance was negligible. Mounted on this stage was a vapor-pressure bulb which was used to calibrate the thermometers against the ^{4}He vapor-pressure scale (T^{58}).[21] The interior of the reservoir on this stage contained copper fins machined directly from the platform. The distance between the fins was about 0.1 cm, sufficiently small to provide fast thermal response. The walls and top of the reservoir were machined from a single piece of beryllium copper and were sealed to the bottom with an indium gasket. The reservoir top served as a capacitative pressure gauge (Sec. II B).[22] The final empty reservoir space was about 10 cm^3 and could be filled by a hole drilled at the center which was connected to three separate inlets as shown in Figs. 1 and 2. One of each of the inlets was connected to the fill capillary, to the hot volume, and to the thermal-conductivity cell. The thermal-conductivity cell (see Sec. II C) was bolted to the bottom of the reservoir platform. Apiezon N grease was used between surfaces to enhance thermal contact.

Most capillaries and all wires coming from room temperature were thermally attached to the top flange of the

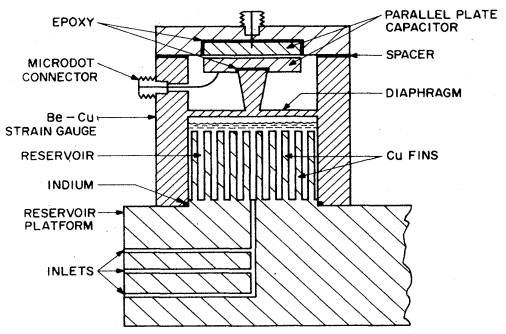

FIG. 2. Schematic diagram of the reservoir and the capacitative pressure gauge.

vacuum can, to the refrigeration stage, and to the isothermal platform. Only the capillary used to fill the vapor-pressure bulb was brought directly from the top of the can to the bulb without touching the refrigeration and isothermal stages. This provided the positive temperature gradient necessary to avoid condensation in the fill line.

The heat conductance between stages was provided primarily by the capillaries filled with ^{4}He II. The conductance between the refrigeration stage and the isothermal stage was about 7×10^{-4} W at the typical operating temperatures of each stage, while the conductance between the isothermal stage and the reservoir was about 5×10^{-5} to 1.5×10^{-4} W, depending on the operating temperature of the reservoir. For the experiments with short cells, which required large currents, extra heat conductance was added by installing copper wires between stages to provide cooling power up to 1 mW at the cell level.

B. Pressure gauge

The detailed structure of the pressure gauge is shown in Fig. 2. It was a capacitive strain gauge of the type described by Straty and Adams.[22] The movable diaphragm was 0.12 cm thick and 2.5 cm in diameter. A copper disc of diameter 2.2 cm was expoxied to a post in the center of the diaphragm and served as the active capacitor plate. A second fixed copper capacitor plate of the same size was held in position with epoxy in a brass holder. Each plate and assembly were lapped flat and gold plated. The distance between the plates was adjusted by spacers with suitable thickness and typically was 0.013 cm. The gauge capacitance varied from 26 to 37 pF over the pressure range 0—28 bars. This capacitor and a similar reference capacitor (45 pF) on the isothermal platform were used in conjunction with a seven-digit ratio transformer[23] and a phase-sensitive lock-in amplifier[24] in an ac bridge arrangement similar to that described by others.[15,16,25] A variable series resistance (a few ohms) was used in the appropriate arm of the bridge to null the out-of-phase component of the signal. A resolution of a few parts in 10^9 in the capacitance was easily achieved and corresponded to a pressure resolution of about 10^{-7} bars.

The gauge was calibrated from 0—25 bars (whole range) using a Texas Instruments (TI) quartz bourdon-tube gauge[26] and from 0—2.6 bars (limited range) using an MKS Instruments baratron gauge.[27] Both TI and MKS gauges had been calibrated previously as discussed in Ref. 17. The calibration data points for our low-temperature pressure gauge were fitted initially to the equation[28]

$$P=A\left[\frac{1}{\mathscr{R}_0}-\frac{1}{\mathscr{R}_p}\right]+C\left[\frac{1}{\mathscr{R}_0}-\frac{1}{\mathscr{R}_p}\right]^3, \qquad (2.1)$$

where P is the pressure in bars, $\mathscr{R}_p$ is the bridge ratio, and A, C, and $\mathscr{R}_0$ are fitting parameters. This revealed that the cubic term was not needed for the fits, indicating great linearity of the gauge. The parameters A for both fits (whole range and limited range) differed from each other by less than 1%, and the deviation $|\delta P|=|P-P^{\rm fit}|$ was less than 0.7×10^{-3} and 20×10^{-3} bars for the limited- and whole-range fits, respectively. For the whole-range fit, δP varied slowly with pressure with $|d(\delta P)/dP|<4\times10^{-3}$ for all P. The limited-range fit was used to calibrate the thermometers discussed below. The pressure gauge was recalibrated after thermal cycles to room temperature, though the parameter A in Eq. (2.1) changed typically by less than 1% upon cycling. The value of A typically was 52 bars.

C. Thermal-conductivity cells

Figures 3(a) and 3(b) show cross sections of the thermal-conductivity cells and illustrate two different designs. The design in Fig. 3(a) is for cells with spacings $d\gtrsim0.1$ cm (cells E and F), while the design in Fig. 3(b) is for shorter cells (cells H and I). The dimensions of the cells measured at room temperature are given in Table I. Also given in Table I are data for cell G, which has a design similar to that shown in Fig. 3(a) and was used in another apparatus intended for nanokelvin thermometry experiments.[13,16]

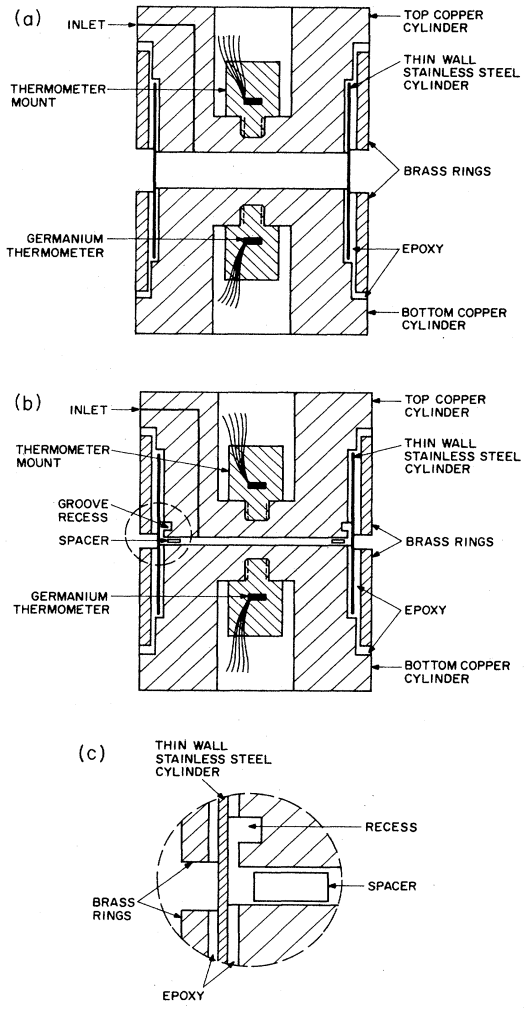

FIG. 3. (a) Schematic diagram of the thermal-conductivity cells with relatively large spacing (cells E and F). (b) Schematic diagram of the thermal-conductivity cells with relatively small spacing (cells H and I). (c) Detail of (b).

TABLE I. Cell parameters. The numbers in parentheses are the uncertainty of the last digit.

Cell	Spacing d (cm)	Area A (cm^2)	Wall thickness d_w (cm)
E	0.4525(6)	18.037	0.0233(5)
F	0.2032(6)	18.047	0.0227(5)
G	0.1011(6)	18.953	0.0127(7)
H	0.0127(6)	17.801	0.0177(5)
I	0.0025(6)	17.765	0.0174(5)

Each cell was made by epoxying two OFHC copper cylinders of radius 2.4 cm into a snugly-fitting stainless-steel tube of wall thickness approximately equal to 0.02 cm using Emerson and Cummings No. 1266 epoxy. The walls were sufficiently thin so that the majority of the heat transport was through the fluid. In order to obtain a flat and parallel geometry, both surfaces of the copper cylinders of each cell were lapped and polished to a mirror finish and coated chemically[29] with 500 Å of gold. The deviation from flatness was 3 to 4 μm. While assembling the cells, a method described in Ref. 30 (Sec. 2.4.2) was used to make the surfaces as parallel as possible. Helium sample was introduced into the cell through a small inlet of diameter 0.034 cm which was drilled, before lapping and gold plating, off center in the top copper cylinder. For the short cells, H and I, three small circular Mylar spacers of the appropriate thickness placed equitriangularly between the surfaces of the cylinders fixed the spacing of the cell. The total area of the Mylar spacers was about 0.5% of the total area of the cell and was taken into account in the data analysis. In order to prevent epoxy from flowing, under the influence of surface tension, into the working area of the short cells, a recess was machined around the cylinder with the filling hole as shown in Fig. 3 (this was not necessary for the tall cells). Since the cells had to withstand pressures up to 30 bars, extra structural support of the walls had to be added. This was done by putting snugly-fit brass rings over the stainless-steel tube and the copper cylinders as shown in Figs. 3(a) and 3(b). The brass rings were epoxied at the time of the cell assembly in such a way that the ends were slightly below the surface level of the copper cylinders.

A 1.6-cm-diam hole, about 2 cm deep, was bored into each cylinder on the side opposite to the active cell surface. Its bottom terminated in a smaller, tapped hole of depth 0.5 cm which, in turn, terminated about 0.2 cm from the lapped, active cell surface as shown in Figs. 1 and 3. A germanium thermometer, mounted together with its reference resistor on a copper post, was screwed into the tapped hole.

The cell was then bolted to the reservoir platform with the end with the fill line upward. The heater, which was composed of six metal-film resistors connected in series with total resistance of 7 kΩ, was mounted on the bottom cylinder as shown in Fig. 1.

D. Thermometry

Roughly calibrated carbon thermometers[31] were used with two leads on all stages and the hot volume, so that the temperature of every stage could be known approximately. Another carbon resistor mounted on the isothermal stage was used in a five-wire ac resistance bridge similar to that shown in Fig. 4 of Ref. 20. The main thermometers mounted on the top and bottom of each cell were germanium thermometers.[32] Five-wire ac resistance bridges[15] were used for these thermometers. Similar to Ref. 17, wire-wound 5-kΩ resistors[33] were used as references and virtually eliminated any thermometer drift. Repeated measurements of the λ-point temperature at SVP indicated that the thermometer systems were stable to about ± 10 μK over periods of several weeks at low temperatures and changed by no more than 50 μK upon cycling between room temperature and 2 K.

The top germanium thermometer was calibrated over the range $1.6 \leq T \leq 4.2$ K against the sample vapor pressure on the 1958 ^{4}He vapor-pressure scale (T^{58}).[21] The calibration was done by preparing a sample at saturated vapor pressure (SVP) in the cell and the reservoir and by measuring its vapor pressures at different temperatures with the capacitative sample pressure gauge. This gauge, in turn, had been calibrated previously against the MKS gauge over the range 0—2.6 bars (see Sec. II B above). During the calibration, the temperature was held constant to about ± 1 μK using a thermometer bridge and electronic regulation. The vapor pressure could then be measured with a resolution corresponding to about 20 μK near 2 K. To check the reliability of this calibration, a separate calibration in the range of 1.6—2.8 K, using the vapor-pressure bulb and a 0—100-Torr MKS Instruments baratron gauge at room temperature, was performed. The two calibrations differed by less than 0.3 mK. The calibration with the sample pressure gauge was adopted for the whole range. The bridge ratio $\mathscr{R}$ and the corresponding temperatures during calibration were fitted, separately over the ranges 1.6 to 2.6 K and 2.6 to 4.2 K, to the equation

$$\log_{10}\left[\frac{T}{T_\lambda}\right] = \sum_{n=1}^{3} A_n \left[\log_{10}\left[\frac{\mathscr{R}(1-\mathscr{R}_\lambda)}{\mathscr{R}_\lambda(1-\mathscr{R})}\right]\right]^n . \quad (2.2)$$

Here the coefficients A_n are fitting parameters, $T_\lambda \equiv 2.172\,000$ K is the temperature at the λ point, and for the temperature range 1.6 to 2.6 K the bridge ratio $\mathscr{R}_\lambda$ at T_λ was determined during calibration with a resolution corresponding to ± 1 μK. For the range 2.6 to 4.2 K, $\mathscr{R}_\lambda$ was treated as an adjustable parameter. The parameters A_n changed less than 0.1% upon cycling to room temperature and it was not necessary to reestablish the temperature scale each time. The deviations $\delta T = T - T^{\text{fit}}$ of T from that given by Eq. (2.2) had a root-mean-square value of about 0.02 mK which was the same as our vapor-pressure resolution. The temperature scale will reproduce exactly the fixed-point value $T_\lambda = 2.172\,000$ K, and the deviations from T^{58} are no more than ± 0.3 mK.

Table II shows the λ-point temperatures obtained with different cells for several pressures. Also shown in Table II are the λ-point temperatures obtained by Kierstead[34] and by Singsaas and Ahlers.[17] The agreement is excellent.

Having calibrated the top thermometer, the bottom thermometer then could be calibrated against it with extremely high resolution over the range of 1.6—2.17 K,

where ^{4}He is superfluid and the thermal conductivity is effectively infinite. In this range there was essentially no temperature difference between the top and bottom thermometers. Above T_λ, the bottom thermometer was calibrated using the shortest cell (I), which in the presence of the thermometer power dissipation of 4×10^{-8} W had negligible temperature differences between the top and the bottom thermometers even above T_λ. The bottom thermometer was used only to measure the temperature differences across the cell which were induced by the heat current.

E. Procedures and data analysis

1. *Pressure regulation*

For measurements at SVP, the cell and the reservoir were filled to slightly above 1 atm at 4.2 K. With the sample-line valve closed, the sample would then be at SVP when cooled somewhat below 4.2 K. For measurements at high pressures, the cell and the reservoir were first filled at a temperature near $T_\lambda(P)$ to the appropriate pressure as indicated by the TI gauge,[26] and then the ac bridge for the pressure gauge was balanced. After closing the sample-line valve the unbalance signal from the bridge was used as input to a temperature controller[35] which increased or decreased the temperature of the hot volume. The temperature changes in the hot volume would result in pressure changes in the cell and the reservoir. The hot volume operated typically in the temperature range 3–4 K. By this method the pressure was held constant to $\pm4\times10^{-6}$ bars, corresponding to a stability of typically 0.05 μK for T_λ. This variation of T_λ was smaller than the resolutions of the germanium thermometry and thus negligible.

2. *Determination of* T_λ

To determine the λ point on our temperature scale, the temperature of the cell was brought slightly below T_λ (usually about 50 μK), and a constant power was dissipated at the bottom of the cell. The total heat input to the system was adjusted so that the cell warmed up very slowly (typically 1.5 μK/min). Both the top and bottom thermometer-bridge unbalances were monitored on a chart recorder. When the temperature of the bottom solid-liquid interface reached T_λ, the bottom thermometer would start to warm up more rapidly because thermal gradients would develop in the normal fluid with finite conductivity. The resulting kink in the warming curve of the bottom thermometer determined the λ point $T_{h\lambda}$ at the bottom of the cell with an accuracy of a few tenths of a μK. The corresponding top temperature $T_{c\lambda}$ was then recorded.

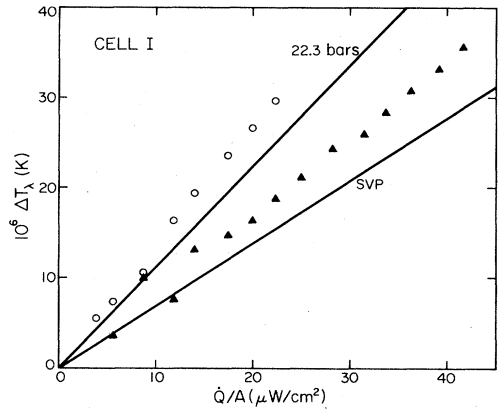

FIG. 4. The temperature difference ΔT_λ between the top and bottom of cell I when the bottom is at the λ point. The solid triangles are results at SVP and open circles are results at 22.3 bars. The solid lines are results obtained from the boundary resistance given by Eq. (2.6).

The measured temperatures $T_{c\lambda}$ and $T_{h\lambda}$ depended upon the current $\dot{Q}$ and, for $\dot{Q}>0$, differed by an amount ΔT_λ equal to the temperature drop due to the boundary resistance[36] (see Sec. V) and due to dissipation (mutual friction) in liquid ^{4}He II. Figure 4 shows results of ΔT_λ at different power densities for cell I at SVP and 22.3 bars (the origin was determined by extrapolation to zero power). The dependence on $\dot{Q}$ is linear within experimental resolution. The solid lines are results obtained from the boundary resistance measurements taken in ^{4}He II discussed below in Sec. V, and they are consistently lower than the measurements using this procedure. The difference is believed to be due to the mutual friction in He II which is negligible well below T_λ but appreciable close to T_λ.[37] We were unable to detect a genuine power dependence[38] of T_λ under our experimental conditions and with the sensitivity of our thermometry.

During the measurement of the thermal conductivity using the tall cells E and F, T_λ was determined with a

TABLE II. λ-point measurements at various pressures. At SVP, $T_\lambda=2.172\,00$ K for each cell by definition.

P (bars)	T_λ (K) Cell E	Cell F	Cell H	Cell I	Ref. 34	Ref. 17
6.95		2.100 94	2.100 92		2.100 98	2.100 30
14.73		2.001 76	2.001 67		2.002 00	2.002 50
22.30	1.892 99	1.893 12	1.893 01	1.892 90	1.892 88	1.893 20
28.00		1.800 58	1.800 41		1.800 65	1.800 34
Upper λ point		1.763 67			1.7633	1.763 34

fixed power density of 0.16 μW/cm^2. In those cases the power dependence was negligible. In the case of the short cells (especially for cell I), larger power densities had to be used in order to obtain accurate T_λ measurements, and an extrapolation to zero power for T_λ was applied in the data analysis. T_λ was determined both before and after each thermal-conductivity measurement when the reduced temperature was small.

The above procedure yielded the λ point at the cell bottom. We did not apply any correction for the effect of the finite sample height in the gravitational field, because this correction is negligible compared to our thermometer resolution.

3. Conductance measurements

During the measurements, the temperature T_c at the top (cold) end of the cell was held fixed by a temperature controller[35] driven by the out-of-balance signal of the cold-end thermometer bridge. Heat was then applied to the heater at the bottom (hot) end. The power $\dot{Q}$ was measured by a four-lead method with an estimated uncertainty of 0.02%. The corresponding change of the temperature ΔT at the bottom thermometer was recorded, and hence the conductance K of the cell could be obtained from the relation

$$K=\dot{Q}/\Delta T\ . \tag{2.3}$$

4. Wall conduction

Close to the λ point, the heat conducted by the walls was small compared to that conducted by the liquid helium, but far away from T_λ the wall conduction could be as large as 10% or so of the total. For cell F the wall conduction was measured in a separate experiment after the measurements of total conductance were finished. At room temperature the cell was flushed repeatedly with pure nitrogen gas, pumped out as well as possible, and sealed. Hence, when the cell was cooled down to liquid-helium temperature where any residual nitrogen gas would be frozen, the cell was empty and the wall conductance K_w could be measured for the whole temperature range (1.5—4.2 K). The results were fitted to the relation

$$K_w=AT+BT^2+CT^3$$

and yielded $A=0.6076$ mW K^{-2}, $B=0.0683$ mW K^{-3}, and $C=-0.00941$ mW K^{-4}. The thermal conductivity of the wall material when estimated using a cross-sectional area to length ratio equal to 1.46 cm (see Appendix A and data in Table I) is consistent with the known thermal conductivity of stainless steel.[39] The wall conduction of other cells was obtained by comparing the dimensions of each cell with cell F (see Table I). To do that, one has to know the circumference, the wall thickness, and the effective thermal length for each cell. The circumference was known very accurately and the wall thickness was measured with 3—4 % accuracy. The effective thermal length was more difficult to obtain with reasonable accuracy, especially for cells H and I which were very short and for which the epoxy did not fill the gap between the wall and the copper cylinder all the way to the active surface [see Fig. 3(c)]. Because of the poor thermal conductivity of stainless steel and the imperfect thermal attachment of the walls to the copper cylinders, the effective thermal length is longer than the spacing of the cell and changes as the thermal conductivity of liquid helium changes. In order to obtain quantitative results, we performed computer simulations of the two-dimensional heat-flow problem for individual cells. Details will be presented in Appendix A. From the simulations the effective thermal length for each cell was calculated at different temperatures and pressures. With such information the wall conduction would be estimated with an accuracy of a few percent. The current $\dot{Q}_w=K_w\,\Delta T$ could then be subtracted from the total current $\dot{Q}$ to yield the current

$$\dot{Q}_l=\dot{Q}-K_w\,\Delta T \tag{2.4}$$

passing through the liquid.

5. Boundary resistance

In addition to the temperature difference ΔT_l across the liquid helium, the current $\dot{Q}_l$ generates a temperature difference ΔT_b between the liquid adjacent to each of the two parallel cell surfaces and the corresponding thermometer. Each of these latter temperature differences is the sum of a contribution ΔT_K due to the Kapitza resistance[40] at the boundary and of $\Delta T_{\rm Cu}$ due to the gradients in the copper between the surface and the thermometer (see Fig. 3). We estimated numerically (see Appendix B) the contribution of $\Delta T_{\rm Cu}$ to ΔT_b, assuming a conductivity of 2 W/cm K for copper and using a Kapitza resistance of about 0.6 K cm^2/W. At SVP we found $\Delta T_{\rm Cu}/\Delta T_b$ to be approximately equal to 0.4. The sum $\Delta T_b=\Delta T_{\rm Cu}+\Delta T_K$ was measured in the superfluid phase, where, for sufficiently small $\dot{Q}_l$, we have $\Delta T_l=0$, and thus $\Delta T_b=\Delta T/2$. The measurements yield the boundary resistance

$$R_b=A\,\Delta T_b/\dot{Q}_l\ . \tag{2.5}$$

The estimates in Appendix B show that the experimental values of R_b are 20% to 40% larger than the contribution from the Kapitza resistance, depending on the pressure and the exact value of the conductivity of copper.

Figure 5(a) shows the results of R_b for all cells measured at SVP. They are smaller than most of the Kapitza resistances reported by others,[36] but agree reasonably with measurements by Johnson and Little[41] (quantitative agreement cannot be expected because R_K depends very much on the conditions of individual surfaces; see Ref. 36). As expected from previous work, R_b varies roughly as T^{-3}. This is shown in Fig. 5(b), where R_bT^3 is plotted against T for cell F. The results differ from a constant by less than 7% for the whole temperature range. Also shown in Fig. 5(b) are results at different pressures. They demonstrate that the boundary resistance is pressure independent within our resolution, except perhaps for $T\lesssim 1.8$ K, where the SVP and 28.0-bars results differ from each other by about 7%. A similar very mild pressure dependence was reported elsewhere.[42]

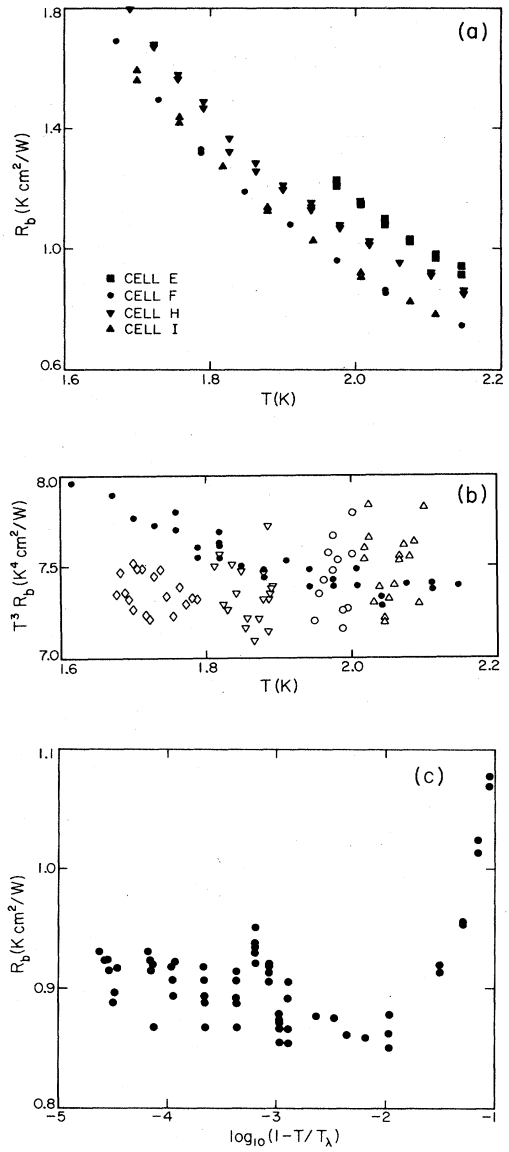

FIG. 5. (a) Boundary resistance of cells E, F, H, and I when filled with ^{4}He II at SVP. (b) Boundary resistance R_b, multiplied by T^3, of cell F at SVP (solid circles), 6.85 bars (open triangles), 14.73 bars (open circles), 22.3 bars (inverted open triangles) and 28.0 bars (open lozenges). (c) Boundary resistance of cell H at SVP close to the λ point.

We wish to estimate R_b for $T > T_\lambda$, where it cannot easily be measured, from the data below T_λ. This would be difficult if R_b had a significant singularity at T_λ. Therefore we made measurements at SVP and for one of the cells (cell H) on the superfluid side with high resolution and quite close to T_λ. The results are shown in Fig. 5(c). They do not reveal any singularity in R_b as T_λ is approached from below. Thus, we fitted the regular function

$$R_b = R_0 T^{-X} \tag{2.6}$$

to the results for R_b at SVP over the entire temperature range [see Fig. 5(a)] but separately for each cell, treating R_0 and X as adjustable parameters. In each case the deviations of the data from the fit were only about 2×10^{-2} K cm^2/W. Equation (2.6) with the parameters for a given cell was then adopted for all pressures and used to extrapolate to $T > T_\lambda$. We must keep in mind, however, that the absence of a noticeable singularity in R_b for $T < T_\lambda$ does not guarantee the applicability of Eq. (2.6) for $T > T_\lambda$.

6. *Thermal-conductivity measurements*

The conductance of the helium is given by

$$K_{\rm He} = \dot{Q}_l / (\Delta T - 2\dot{Q}_l R_b / A) , \tag{2.7}$$

where $\dot{Q}_l$ is obtained from Eq. (2.4), R_b is given by Eq. (2.6), A is the cross-sectional area of the cell (see Table I), and ΔT is the measured temperature difference caused by the imposed current $\dot{Q}$. The factor of 2 in Eq. (2.7) reflects the boundary-resistance contribution to ΔT at *both* ends of the (symmetric) cells. The average thermal conductivity $\bar{\lambda}$ of the helium over the temperature range spanned by ΔT is obtained from

$$\bar{\lambda} = K_{\rm He} d / A , \tag{2.8}$$

where d is the cell spacing (see Table I as well as Tables XIII and XIV below).

We chose to assign each measured value of $\bar{\lambda}$ to a temperature

$$\bar{T} = T_c + \Delta T/2 \tag{2.9a}$$

with the corresponding reduced temperature

$$t = \bar{T}/T_\lambda - 1 . \tag{2.9b}$$

Here T_c is the cold-end temperature. Since the conductivity near T_λ is nonlinear and varies significantly over the range $T_c \le T \le T_c + \Delta T$, a curvature correction, consistent with the choice of Eq. (2.9), must be applied to the values of $\bar{\lambda}$ given by Eq. (2.8) in order to obtain the conductivity λ at the temperature t. This correction is discussed in Appendix C. It is negligible whenever $\Delta T \ll \bar{T} - T_\lambda$, but, for $\bar{T}$ near T_λ where ΔT was often of the same size as $\bar{T} - T_\lambda$, the correction could become as large as 10% or so.

7. *Power dependence of the conductivity*

We searched extensively for a dependence of the measured conductivity in cells F and H upon $\dot{Q}_l$ but found none for values of $\dot{Q}_l/A$ covering the range 0.04 to 40 μW/cm^2. In order to display the data, we fitted to them, separately for each cell, the empirical function

$$\lambda = a t^{-x}(1 + b t^y) , \tag{2.10}$$

where a, b, x, and y are adjustable parameters. The deviations of the individual measurements, in percent, are plotted in Fig. 6(a) for cell F and in Fig. 6(b) for cell H at SVP. The systematic deviations from the fit are, of course, not significant. Of importance is the fact that the

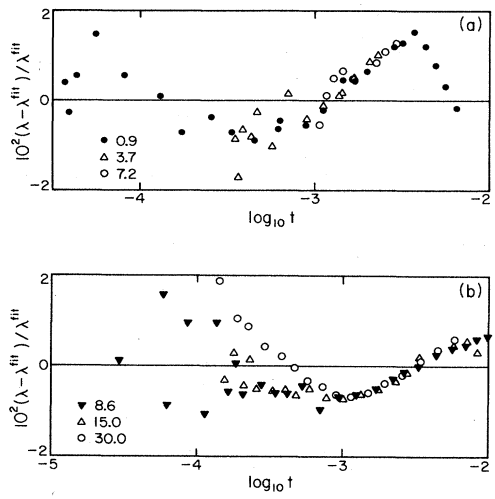

FIG. 6. Deviations of the thermal conductivity λ measured at various heat current densities from a fit of cell-F conductivity data to Eq. (2.10). (a) Deviations of cell-F data over the range 0.9 to 7.2 μW/cm^2. (b) Deviations of cell-H data over the range 8.6 to 30.0 μW/cm^2. The current densities in μW/cm^2 are given in the figures.

results show no power dependence for the power-density range used. The slight differences for cell H at t smaller than $10^{-3.5}$ may be attributed to the large uncertainties in the measurements at low power [as evident from the scatter of these measurements in Fig. 6(b)] and the large curvature corrections for the high-power measurements. In any case, the difference is less than 0.4%.

For a given power level, the point with the smallest t in Figs. 6(a) and 6(b) corresponds to a cold-end temperature T_c only a few μK above T_λ. The value of the smallest t is thus determined primarily by the size of ΔT [see Eqs. (2.9)]. Although for a given power level and a given cell height it is not possible to obtain data at values of t significantly smaller than those shown in Fig. 6, it should be kept in mind that the measurements probe the entire reduced-temperature range from about 10^{-6} to $2t$.

F. Errors

Errors in λ arise from uncertainties in the power, the cell dimensions, the measurement of ΔT, the wall conductance, and the boundary resistance. Errors in the power are always much less than 0.1% and may be neglected. Errors in the cell dimensions contribute no more than 0.2%, except in the case of the short cells H and I, where the direct measurement of the spacing d has a larger relative error. For those short cells, more accurate values of d were obtained by comparing λ at large t, well away from the singularity near T_λ, with absolute measurements of λ based on the directly measured cell dimension in cell F. This comparison is discussed in Appendix D.

At large t, errors in λ due to uncertainties in ΔT could readily be kept below 0.1%. For small t, errors from this source were limited by the temperature resolution of 10^{-7} K. Since $\Delta T < 2tT_\lambda$ [see Eqs. (2.9)], it follows that, e.g., at $t=10^{-5}$, the uncertainty in λ from the temperature measurement cannot be less than $\frac{1}{4}$% and more typically will be $\frac{1}{2}$%. For each data point the probable error from this source can be estimated from ΔT.

The wall conductance of cell F was measured with an accuracy of about 0.1% when the cell was empty. As shown in Appendix A, however, the effective thermal length of this cell changes when the cell is filled with He I by an amount which depends upon t and reaches about 10% at small t. We think that the simulation in Appendix A predicts this *change* in the thermal length with an accuracy of 10% and, thus, conclude that we know the wall conduction of cell F with systematic errors which are no larger than 1% near T_λ and smaller further away. Since the wall conduction contributes only 10% to the total conduction well above T_λ and less close to T_λ, errors in λ for cell F due to errors in wall conduction are below the 0.1% level and may be neglected.

The uncertainty in the wall conductance of the other cells is attributable primarily to the uncertainty in the wall thickness which was typically 3% to 4%. For cells E and G this leads to an uncertainty in λ of 0.3% to 0.4% at large t and less near T_λ. For cells H and I the effective thermal length (see Appendix A) is much larger than the actual cell length, and the contribution of K_w to K is thus significantly reduced. Therefore, the uncertainty in λ due to the uncertainty in K_w is near or below the 0.1% level in these cases.

The boundary resistances were measured below T_λ with a precision of about 5%. However, for cells H and I these results could be systematically low by about 10% because of the ill-defined active cross-sectional area due to the recess cut on the top copper cylinder [in computing R_b from Eq. (2.5) we used only the flat cross-sectional area A given in Table I and did not include the area of the recess]. The effect of the uncertainties in R_b upon λ can be estimated from the data in Table III which give the relative contribution of the temperature drop $2\Delta T_b$ [see Eq. (2.5)] across the boundaries to ΔT for cell F at several temperatures and at the two extreme pressures. For cell F (on which our main measurements are based), the uncertainty in λ due to the uncertainty in R_b is only 0.1% even quite close to T_λ, provided the extrapolation to $T > T_\lambda$ of the measurements below T_λ, using Eq. (2.6), is valid. It can be seen that the effect of R_b for cell F is negligible for large t.

TABLE III. The ratio of the temperature drop $2\Delta T_b = 2\dot{Q}_l R_b/A$ [Eq. (2.5)] associated with the boundaries to the total temperature drop ΔT at several reduced temperatures for cell F. Estimates of R_b are based on an extrapolation of Eq. (2.6) to $T > T_\lambda$.

P	SVP	28 bars
t		
10^{-6}	0.0245	0.0165
10^{-5}	0.0138	0.0107
10^{-4}	0.0048	0.0041
10^{-3}	0.0019	0.0023
10^{-2}	0.0010	0.0019

For the other cells, $2\Delta T_b/\Delta T$ can be estimated from the cell-F results in Table III by multiplying by the inverse of the cell-spacing ratio (see Table I). In the case of cell H, for instance, a 5% error in R_b will lead to a 1% error in λ if $t=10^{-5}$. For the extreme case of cell I, errors due to R_b are even much larger and our measurements only have the value of showing that no *dramatic* changes in λ occur as d is decreased.

The overall uncertainty of the cell-F data, as determined by the above sources of errors, is a few tenths of 1% over most of the temperature range. Because of temperature resolution limitations and uncertainties in the boundary-resistance extrapolation to $T>T_\lambda$, it increases as the smallest values of t are approached [see Sec. III C 2(c) below].

III. RESULTS

A. Range of measurements

We measured the thermal conductivity in five cells of different spacing d (see Table I), but our major results were obtained with cell F which had $d=0.203$ cm. For larger d (cell E), the precision of the measurements deteriorates because of long thermal relaxation times, and measurements at low P are restricted to small values of t because of convection (see below) unless heating is done from above. For smaller d (cells G, H, and I), systematic errors due to the boundary-resistance correction become significant at small t (see Secs. II E 5 and II F), and systematic errors due to the uncertainty in the directly measured cell spacing are no longer negligible. Thus a value of d near 0.2 cm is the optimum choice. Measurements in cells other than cell F primarily served the purpose of ruling out the existence of anomalously large size effects upon λ and of exploring the influence of the boundary resistance on the measurements at small t.

TABLE IV. A list for each cell (For cell G, data were taken only at SVP) of the isotherms and isobars along which measurements were made.

Isobar (bars)	Cell E	F	H	I
SVP	yes	yes	yes	yes
6.85		yes	yes	
14.73		yes	yes	
22.30	yes	yes	yes	yes
28.00		yes	yes	
Isotherm (K)	**Cell E**	**F**	**H**	**I**
2.0999		yes		
2.2278	yes	yes		yes
2.3170		yes		
2.4237		yes		
2.6257		yes		
2.8219		yes		
3.0144		yes		
3.3015	yes	yes	yes	yes
3.5913		yes		

For each cell, Table IV lists the isotherms and isobars along which measurements were made. The isotherms covered the temperature region well away from T_λ and the pressure range from near SVP to 30 bars. For P greater than SVP, the isobars spanned a wide range of the reduced temperature from $t\simeq 2\times 10^{-6}$ on up to near $t=0.1$. At larger t, isobar data were difficult to obtain because the "hot-volume" technique (see Sec. II E 1) did

TABLE V. Thermal conductivity results for cell E.

t	λ (ergs/s cm K)	$\hat{R}_\lambda$	$\dot{Q}_l/A$ (ergs/s cm^2)	$10^3\Delta T$ (K)
		P equals SVP		
0.000 003 1	30 285	0.3025	0.749	0.0103
0.000 003 7	27 641	0.2927	0.748	0.0114
0.000 005 6	23 564	0.2928	0.976	0.0174
0.000 006 0	23 322	0.2972	1.102	0.0196
0.000 007 4	21 000	0.2903	1.376	0.0265
0.000 009 7	18 915	0.2900	1.523	0.0331
0.000 011 9	17 531	0.2914	1.841	0.0426
0.000 015 0	15 812	0.2867	2.189	0.0555
0.000 018 7	14 191	0.2806	2.567	0.0715
0.000 025 0	12 399	0.2744	1.833	0.0639
0.000 029 1	11 464	0.2692	2.179	0.0813
0.000 037 6	10 291	0.2671	3.401	0.1343
0.000 044 4	9670	0.2678	3.397	0.1460
0.000 053 9	8782	0.2624	4.357	0.1993
0.000 065 9	8069	0.2610	5.152	0.2526
0.000 080 2	7423	0.2596	6.013	0.3160
0.000 151 2	5710	0.2574	4.557	0.3483
0.000 183 6	5236	0.2552	5.937	0.4886
0.000 206 5	4934	0.2523	1.479	0.1349

TABLE V. (*Continued*).

t	λ (ergs/s cm K)	$\hat{R}_\lambda$	$\dot{Q}_l/A$ (ergs/s cm^2)	$10^3\Delta T$ (K)
0.000 251 2	4510	0.2497	3.316	0.3286
0.000 322 0	4075	0.2498	5.873	0.6357
0.000 426 2	3641	0.2506	9.137	1.0879
0.000 514 6	3404	0.2533	5.819	0.7621
0.000 632 4	3138	0.2546	9.057	1.2731
0.000 831 4	2815	0.2563	3.235	0.5174
0.001 068 1	2584	0.2617	8.940	1.5449
0.001 470 0	2329	0.2706	17.411	3.2890
0.001 885 0	2159	0.2795	1.409	0.2945
0.002 259 7	2055	0.2881	8.777	1.9210
0.002 719 8	1957	0.2978	17.138	3.9178
0.003 418 6	1852	0.3122	1.390	0.3386
0.004 711 4	1738	0.3387	0.345	0.0896
0.006 398 2	1642	0.3683	0.124	0.0340
		$P=22.30$ bars		
0.000 009 5	9048	0.2101	0.742	0.0319
0.000 011 4	8583	0.2147	0.241	0.0126
0.000 015 1	7529	0.2105	0.456	0.0266
0.000 016 6	7082	0.2055	0.964	0.0541
0.000 022 2	6352	0.2066	1.218	0.0750
0.000 030 5	5447	0.2012	1.212	0.0915
0.000 036 5	5328	0.2115	0.839	0.0690
0.000 041 5	4983	0.2084	1.346	0.1137
0.000 050 9	4594	0.2086	1.641	0.1486
0.000 067 3	4150	0.2111	2.138	0.2109
0.000 081 4	3834	0.2108	2.129	0.2331
0.000 110 4	3437	0.2142	2.887	0.3461
0.000 151 3	3069	0.2179	3.753	0.4985
0.000 204 4	2771	0.2232	1.451	0.2345
0.000 295 5	2502	0.2354	3.249	0.5735
0.000 376 2	2338	0.2439	4.661	0.8724
0.000 467 8	2195	0.2514	1.429	0.2932
0.000 571 8	2093	0.2615	3.206	0.6867
0.000 724 8	2001	0.2771	5.684	1.2654
0.000 984 5	1883	0.2984	1.413	0.3384
0.001 476 0	1795	0.3406	8.801	2.1972
0.002 064 7	1732	0.3824	17.208	4.4237
0.002 811 5	1665	0.4232	1.398	0.3788
0.003 782 5	1639	0.4776	14.747	4.0511
0.005 108 1	1615	0.5413	5.576	1.5572
0.008 103 0	1572	0.6542	5.561	1.5964
0.013 101 4	1551		5.552	1.6147
0.021 478 1	1551		5.547	1.6135
0.033 323 7	1552		5.540	1.6104
0.050 310 5	1575		3.116	0.8925
0.076 542 9	1608		1.384	0.3883
0.112 935 3	1654		1.383	0.3772
0.152 872 3	1722		1.382	0.3621

not have sufficient range to hold the pressure constant and the sample-line valve would have had to be opened. For $t>0.1$, the thermal conductivity on any isobar can be obtained with an accuracy of a few tenths of 1% by interpolation along isotherms.

At SVP the largest accessible value of t for cells E and F was 0.006 and 0.018, respectively, i.e., considerably less than 0.1. For these cells this high-temperature limit was set by the onset of convection.[30] Sufficiently close to T_λ, the expansion coefficient of the fluid is negative and heating from below results in a gravitationally stable density gradient. However, at higher T the expansion coefficient is positive and the density gradient is unstable. Convection *actually* occurs at a value of t which at a given temperature depends upon the cell spacing d, the temperature difference ΔT, and the pressure. Thus, e.g., for cell F at

TABLE VI. Thermal-conductivity results for cell F.

t	λ (ergs/s cm K)	$\hat{R}_\lambda$	$\dot{Q}_l/A$ (ergs/s cm^2)	$10^3\Delta T$ (K)
		P equals SVP		
0.000 003 0	33 056	0.3241	1.404	0.0082
0.000 003 5	30 978	0.3238	1.714	0.0105
0.000 004 8	26 277	0.3079	2.238	0.0158
0.000 005 7	24 171	0.3035	2.624	0.0199
0.000 006 8	22 561	0.3019	2.621	0.0218
0.000 009 4	19 357	0.2934	3.484	0.0330
0.000 011 0	17 914	0.2889	3.961	0.0401
0.000 014 7	15 903	0.2867	5.007	0.0560
0.000 019 4	14 186	0.2846	6.174	0.0762
0.000 024 7	12 754	0.2808	6.164	0.0881
0.000 031 3	11 468	0.2769	7.448	0.1166
0.000 037 1	10 673	0.2756	9.614	0.1527
0.000 043 5	9968	0.2739	9.599	0.1694
0.000 055 5	9035	0.2732	9.581	0.1945
0.000 075 2	7877	0.2685	2.389	0.0611
0.000 081 8	7554	0.2663	9.536	0.2405
0.000 115 1	6500	0.2625	7.695	0.2336
0.000 150 0	5778	0.2596	11.463	0.3847
0.000 198 1	5118	0.2573	15.956	0.5931
0.000 228 3	4807	0.2560	18.471	0.7239
0.000 307 6	4231	0.2545	13.484	0.6292
0.000 390 9	3823	0.2538	13.424	0.6978
0.000 461 2	3578	0.2544	18.221	1.0025
0.000 587 4	3238	0.2546	18.130	1.1110
0.000 785 4	2906	0.2582	18.003	1.2375
0.000 926 6	2730	0.2602	13.174	0.9714
0.001 007 1	2656	0.2623	29.618	2.1992
0.001 291 9	2452	0.2695	72.009	5.1961
0.001 594 3	2284	0.2748	23.146	2.0358
0.002 261 7	2067	0.2898	12.924	1.2640
0.002 542 7	2002	0.2957	70.541	6.8796
0.003 720 7	1836	0.3215	8.884	0.9789
0.004 425 2	1766	0.3345	12.743	1.4597
0.005 605 6	1691	0.3569	8.815	1.0549
0.006 460 7	1655	0.3729	8.795	1.0757
0.009 837 5	1554	0.4265	1.401	0.1825
0.010 865 1	1528	0.4395	1.399	0.1853
0.013 575 0	1489	0.4762	0.224	0.0305
0.018 401 2	1440	0.5334	0.088	0.0123
		P=6.85 bars		
0.000 005 5	18 889	0.2670	1.876	0.0183
0.000 007 8	16 249	0.2629	2.229	0.0254
0.000 009 7	14 909	0.2626	2.818	0.0342
0.000 011 5	13 828	0.2605	3.248	0.0420
0.000 015 3	12 256	0.2578	3.949	0.0571
0.000 017 6	11 715	0.2599	3.945	0.0613
0.000 023 5	10 304	0.2562	4.984	0.0864
0.000 030 9	9183	0.2541	6.143	0.1175
0.000 036 6	8520	0.2520	6.926	0.1415
0.000 043 0	7956	0.2507	7.756	0.1684
0.000 059 1	6907	0.2469	9.550	0.2357
0.000 076 7	6230	0.2471	9.516	0.2761
0.000 125 1	5022	0.2425	13.630	0.4788
0.000 156 0	4594	0.2427	15.936	0.6071
0.000 192 6	4203	0.2420	18.456	0.7619
0.000 227 7	3899	0.2404	3.364	0.1741
0.000 282 9	3612	0.2436	23.979	1.1400

TABLE VI. (*Continued*).

t	λ (ergs/s cm K)	$\hat{R}_\lambda$	$\dot{Q}_l/A$ (ergs/s cm^2)	$10^3\Delta T$ (K)
0.000 382 9	3189	0.2439	13.333	0.8245
0.000 470 0	2966	0.2473	18.094	1.1899
0.000 627 0	2682	0.2526	15.493	1.1494
0.000 780 7	2500	0.2584	5.843	0.4723
0.000 859 3	2434	0.2622	26.354	2.1237
0.001 007 8	2328	0.2687	32.837	2.7466
0.001 279 2	2186	0.2797	44.029	3.8854
0.001 639 7	2057	0.2935	12.958	1.2723
0.002 329 8	1914	0.3192	12.882	1.3609
0.002 591 6	1876	0.3282	22.859	2.4593
0.003 283 7	1802	0.3510	22.783	2.5539
0.004 312 0	1731	0.3819	22.693	2.6502
0.005 951 4	1663	0.4260	8.835	1.0751
0.006 964 4	1637	0.4514	8.821	1.0906
0.008 992 4	1600	0.4978	8.799	1.1131
0.011 362 5	1575	0.5480	8.784	1.1284
0.014 759 5	1551	0.6116	8.767	1.1440
0.018 511 7	1537		8.755	1.1528
0.023 312 7	1527		8.744	1.1591
0.029 355 8	1522		8.735	1.1617
0.033 701 8	1520		8.730	1.1623
0.046 005 1	1524		8.720	1.1578
0.056 616 0	1535		5.581	0.7357
0.071 144 2	1549		5.577	0.7285
0.089 723 8	1569		5.573	0.7188
0.112 675 7	1600		5.571	0.7045
		$P=14.73$ bars		
0.000 002 8	20 673	0.2623	0.994	0.0089
0.000 003 8	17 720	0.2526	1.256	0.0129
0.000 005 0	15 936	0.2511	1.548	0.0174
0.000 005 5	15 474	0.2541	1.707	0.0196
0.000 007 2	13 590	0.2475	2.044	0.0263
0.000 009 2	12 171	0.2438	2.412	0.0343
0.000 010 2	11 734	0.2439	1.700	0.0276
0.000 014 1	10 399	0.2454	2.405	0.0431
0.000 019 4	9247	0.2474	1.944	0.0412
0.000 020 2	8897	0.2420	2.398	0.0518
0.000 031 2	7401	0.2391	3.441	0.0882
0.000 033 2	7239	0.2398	4.038	0.1038
0.000 042 2	6587	0.2400	4.673	0.1320
0.000 060 6	5594	0.2357	4.009	0.1397
0.000 067 9	5319	0.2346	4.644	0.1689
0.000 095 6	4588	0.2325	3.394	0.1475
0.000 111 9	4286	0.2316	4.609	0.2126
0.000 152 8	3740	0.2297	4.583	0.2442
0.000 175 1	3549	0.2306	5.974	0.3330
0.000 215 3	3276	0.2319	5.951	0.3615
0.000 254 4	3059	0.2322	5.934	0.3873
0.000 347 3	2775	0.2401	5.899	0.4267
0.000 403 0	2638	0.2431	13.254	0.9810
0.000 600 8	2358	0.2578	13.147	1.1086
0.000 785 8	2207	0.2710	13.089	1.1873
0.000 958 2	2112	0.2828	5.797	0.5547
0.001 141 6	2033	0.2941	13.004	1.2876
0.001 552 0	1925	0.3192	8.992	0.9442
0.001 788 4	1877	0.3317	17.587	1.8889
0.002 058 5	1842	0.3468	8.960	0.9839
0.002 562 9	1783	0.3710	8.936	1.0136

TABLE VI. (*Continued*).

t	λ (ergs/s cm K)	$\hat{R}_\lambda$	$\dot{Q}_l/A$ (ergs/s cm^2)	$10^3\Delta T$ (K)
0.003 165 6	1739	0.3986	8.916	1.0376
0.004 827 1	1671	0.4663	8.884	1.0759
0.005 994 6	1644	0.5082	8.870	1.0918
0.007 162 5	1625	0.5468	8.859	1.1031
0.008 832 4	1607	0.5977	8.849	1.1142
0.012 179 5	1856	0.6883	8.835	1.1274
0.014 361 2	1578	0.7413	8.828	1.1326
0.019 415 0	1570		8.820	1.1368
0.022 291 7	1568		8.816	1.1377
0.030 123 9	1568		8.809	1.1371
0.035 270 2	1573		8.807	1.1329
0.042 080 6	1577		5.635	0.7232
0.050 802 2	1587		5.634	0.7183
0.072 122 8	1614		5.630	0.7062
0.086 658 4	1634		5.632	0.6974
0.105 214 9	1656		5.629	0.6877
		$P=22.30$ bars		
0.000 002 8	16 882	0.2446	0.760	0.0083
0.000 003 8	13 795	0.2248	0.991	0.0127
0.000 004 5	13 132	0.2277	0.758	0.0111
0.000 006 1	11 471	0.2245	0.989	0.0163
0.000 007 7	10 444	0.2238	1.249	0.0223
0.000 009 6	9633	0.2249	1.541	0.0294
0.000 012 0	8770	0.2237	1.861	0.0384
0.000 013 6	8216	0.2202	2.032	0.0445
0.000 018 5	7279	0.2205	2.027	0.0523
0.000 020 4	6927	0.2181	2.205	0.0594
0.000 031 3	5869	0.2190	2.382	0.0779
0.000 038 0	5478	0.2211	2.983	0.1033
0.000 044 6	5015	0.2158	3.417	0.1280
0.000 054 9	4579	0.2145	4.124	0.1671
0.000 073 2	4102	0.2159	6.048	0.2584
0.000 092 3	3741	0.2166	3.379	0.1780
0.000 111 0	3492	0.2181	5.999	0.3237
0.000 138 0	3216	0.2198	9.372	0.5030
0.000 180 1	2936	0.2242	9.311	0.5845
0.000 245 7	2648	0.2305	9.247	0.6703
0.000 290 9	2490	0.2327	9.210	0.7195
0.000 335 6	2401	0.2385	9.187	0.7513
0.000 475 8	2211	0.2551	9.136	0.8234
0.000 550 8	2126	0.2612	9.111	0.8572
0.000 765 4	1987	0.2818	9.062	0.9174
0.000 904 2	1933	0.2950	9.047	0.9429
0.001 016 3	1887	0.3033	36.461	3.5819
0.001 466 5	1803	0.3410	8.997	1.0086
0.001 715 0	1765	0.3583	8.978	1.0282
0.002 351 2	1710	0.4005	8.955	1.0592
0.002 919 7	1676	0.4333	8.939	1.0794
0.003 751 4	1648	0.4783	8.925	1.0962
0.004 582 9	1626	0.5180	8.915	1.1094
0.005 912 4	1605	0.5761	8.904	1.1224
0.007 242 3	1592	0.6287	8.896	1.1307
0.008 906 3	1581	0.6882	8.889	1.1380
0.010 905 5	1573	0.7538	8.884	1.1429
0.015 414 8	1564	0.8827	8.875	1.1487
0.018 264 3	1563		8.872	1.1489
0.021 626 9	1562		8.868	1.1493
0.026 358 3	1564		8.866	1.1469

TABLE VI. (*Continued*).

t	λ (ergs/s cm K)	$\hat{R}_\lambda$	$\dot{Q}_l/A$ (ergs/s cm^2)	$10^3\Delta T$ (K)
0.032 296 6	1569		8.863	1.1430
0.046 005 3	1585		8.859	1.1315
0.054 673 3	1593		8.856	1.1248
0.064 300 0	1609		8.855	1.1139
0.088 365 9	1639		8.850	1.0929
		P=28.00 bars		
0.000 003 2	12 504	0.2141	0.388	0.0061
0.000 003 9	11 243	0.2097	0.557	0.0095
0.000 004 5	10 839	0.2127	0.653	0.0114
0.000 006 3	9403	0.2109	0.868	0.0172
0.000 007 6	8525	0.2058	1.048	0.0225
0.000 009 9	7727	0.2071	1.316	0.0306
0.000 012 5	6989	0.2057	1.535	0.0393
0.000 015 7	6329	0.2042	1.854	0.0515
0.000 019 7	5826	0.2060	2.203	0.0659
0.000 021 7	5562	0.2045	1.236	0.0434
0.000 029 7	4904	0.2046	1.840	0.0719
0.000 038 3	4410	0.2041	3.419	0.1324
0.000 048 0	4022	0.2042	2.963	0.1375
0.000 055 5	3828	0.2063	3.397	0.1643
0.000 073 9	3386	0.2056	1.500	0.0888
0.000 090 3	3145	0.2076	2.336	0.1475
0.000 112 1	2917	0.2109	3.353	0.2259
0.000 151 5	2659	0.2184	3.337	0.2495
0.000 172 2	2583	0.2240	9.317	0.6132
0.000 240 4	2335	0.2337	9.229	0.7387
0.000 307 6	2189	0.2437	9.178	0.8098
0.000 349 2	2130	0.2507	9.161	0.8400
0.000 467 5	1994	0.2668	9.110	0.9067
0.000 596 7	1906	0.2842	9.077	0.9527
0.000 756 5	1840	0.3050	9.052	0.9888
0.000 966 2	1775	0.3286	9.026	1.0249
0.001 258 7	1719	0.3590	9.003	1.0576
0.001 480 0	1690	0.3802	8.990	1.0751
0.001 986 8	1647	0.4246	8.971	1.1017
0.002 272 6	1632	0.4479	8.964	1.1113
0.003 162 0	1596	0.5117	8.947	1.1343
0.003 831 8	1580	0.5548	8.939	1.1449
0.004 668 0	1568	0.6049	8.932	1.1526
0.005 839 4	1553	0.6665	8.924	1.1629
0.007 344 7	1545	0.7400	8.919	1.1680
0.009 019 1	1538	0.8125	8.914	1.1729
0.015 230 0	1529	1.0353	8.904	1.1784
0.017 755 9	1530		8.902	1.1779
0.020 793 8	1529		8.899	1.1778
0.028 420 1	1535		8.896	1.1727
0.033 872 0	1544		8.896	1.1664
0.040 723 2	1549		8.892	1.1622
0.056 290 3	1567		8.888	1.1481
0.065 031 2	1579		8.887	1.1390
0.089 890 9	1613		8.887	1.1148

SVP, measurements with meaningful values of ΔT were limited to $t \lesssim 0.018$, whereas for the same cell at a pressure of a few bars measurements were possible up to $t \simeq 1$. Therefore, at SVP and large t, we obtained some estimates of λ by extrapolation of cell-F isotherm data from higher pressures. These estimates agreed well with cell-H data which, although more precise than the extrapolated cell-F data, were based on values of d obtained by normalizing to cell-F data in a P-T region away from T_λ where data for both cells exist (see Appendix D).

TABLE VII. Thermal-conductivity results for cell H.

	P equals SVP		
t	λ (ergs/s cm K)	$\dot{Q}_l/A$ (ergs/s cm^2)	$10^3\Delta T$ (K)
0.010 917 1	1533	235.443	1.9749
0.015 081 1	1483	150.532	1.3052
0.017 258 0	1467	150.483	1.3197
0.023 830 3	1437	150.388	1.3456
0.026 216 9	1432	234.938	2.1105
0.038 076 3	1416	150.283	1.3649
0.043 955 9	1413	150.267	1.3677
0.050 808 2	1413	150.241	1.3672
0.069 633 7	1423	234.640	2.1208
0.088 661 9	1436	150.145	1.3443
0.103 639 0	1451	234.529	2.0791
0.139 259 9	1484	84.388	0.7314
0.177 328 3	1522	84.350	0.7126
0.212 130 9	1556	234.223	1.9362
0.273 721 5	1611	84.224	0.6724
0.341 928 6	1670	84.140	0.6482
0.417 785 6	1725	233.482	1.7404
0.571 919 7	1819	83.800	0.5925
0.649 024 5	1855	232.463	1.6115
0.733 571 4	1885	83.524	0.5698

The complete tabulation of our experimental data is available elsewhere.[43,44] In this paper we present in numerical form only some of our isobar results for cells E, F, and H in Tables V to VII. For this purpose we selected about 10 points per decade from the complete set of measurements. In each one-tenth decade, the point with the largest ΔT was chosen, except that usually points with ΔT much in excess of 10^{-3} K were avoided. We feel that these subsets provide a fair representation of all our measurements, and the analysis in a subsequent paper will be based upon them. In the various figures we usually show as many data points as possible, however.

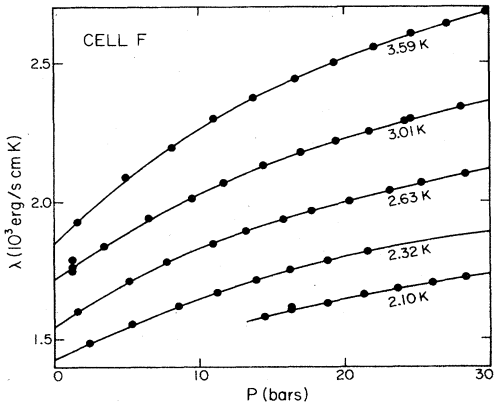

FIG. 7. Results for λ obtained in cell F on five isotherms at the indicated temperatures. The solid lines are fits given by Eq. (3.1).

TABLE VIII. Parameters for Eq. (3.1) giving the thermal conductivity λ in ergs s^{-1} cm^{-1} K^{-1} as a function of the pressure in bars at several temperatures.

T (K)	a	b	c	10^2d
2.0999	1282.3	30.16	−0.7949	0.995
2.2278	1424.8	17.64	−0.0304	0.358
2.3170	1426.8	25.78	−0.3817	0.013
2.4237	1475.9	28.26	−0.5142	0.042
0.6257	1545.3	36.22	−0.9072	1.126
2.8219	1641.4	37.02	−0.8716	1.025
3.0144	1716.9	38.08	−0.7914	0.793
3.3015	1760.8	54.26	−1.6569	2.377
3.5913	1848.0	51.80	−1.1832	1.287

B. Isotherms

Figure 7 shows some of the cell-F results obtained along isotherms. Note that even at 3.59 K the data extend to pressures as low as about 1.5 bars, and extrapolation to SVP (0.5 bar) is not difficult. At the lowest temperature of 2.10 K the data are only for $P \gtrsim 14$ bars. For smaller P the λ line would be approached closely and then crossed. The solid lines in Fig. 7 are fits of the polynomial

$$\lambda = a + bP + cP^2 + dP^3 \tag{3.1}$$

to the data. The least-squares adjusted values of a, b, c, and d are given in Table VIII. Deviations of the data from the fits are at most a few tenths of 1%, as illustrated for three isotherms by the solid circles in Figs. 8(a) to 8(c).

Also plotted in Figs. 8(a) and 8(c) as solid squares are the deviations of cell-E data from the fit of Eq. (3.1) to the cell-F data. The larger scatter for cell E, caused in part by the larger thermal relaxation time for the cell and in part by the use of smaller values of ΔT dictated by the need to avoid convection, is evident. No systematic differences between the two cells are apparent.

In Figs. 8(a) to 8(c) we also show the deviations of the measurements by Kerrisk and Keller[6] from the fit of Eq. (3.1) to cell-F data. Those results have a scatter comparable to that of the cell-E data. We consider the agreement between all three sets of measurements extremely good. Since each set is an absolute measurement involving no normalizations or adjustments, the comparison provides a test of the geometrical factors for each cell, the wall-conductance corrections and the temperature scales over a wide range of T and P.

C. Isobars

Figure 9 shows measurements of λ at SVP and at 22.3 bars (other isobars were omitted for clarity) on logarithmic scales. The direct measurements are given by circles. The triangles represent interpolations or extrapolations based upon Eq. (3.1) and Table VIII. On a more expanded scale, but over a narrower range of t, data for 6.85 and 28.0 bars are shown in Fig. 10. Again, the circles are direct measurements and the triangles were derived from Eq. (3.1).

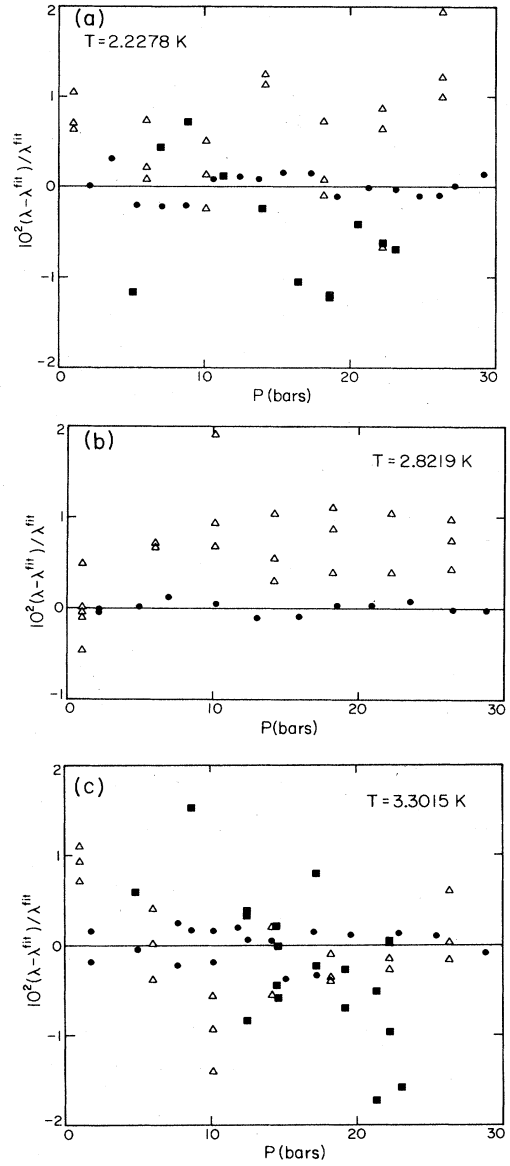

FIG. 8. Deviations of λ in percent of cell E (solid squares), cell F (solid circles), and measurements from Ref. 6 (open triangles) from Eq. (3.1) using parameters given in Table VIII at three temperatures.

1. *Large t*

In order to obtain a closed-form expression suitable, for instance, for the detailed comparison of data from different sources at relatively large t, we fitted the so-called "high-temperature expansion"[45] in the form[5]

$$\lambda=\lambda_\infty(T)(1+\lambda_1 t^{-\nu(1+\eta^4)}) \tag{3.2a}$$

with[5,17] $\nu=0.672$, $\eta^4=0.0145$, and[5]

$$\lambda_\infty(T)=\lambda_{\infty 0}+\lambda_{\infty 1}t+\lambda_{\infty 2}t^2 \tag{3.2b}$$

to the data, least-squares adjusting $\lambda_{\infty 0}$, $\lambda_{\infty 1}$, $\lambda_{\infty 2}$, and λ_1 and using data for $t_m \le t \le 1$ (the choice of t_m is discussed

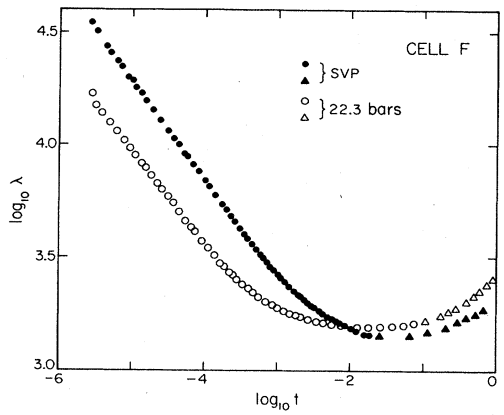

FIG. 9. Thermal conductivity λ at SVP (solid symbols) and 22.3 bars (open symbols) obtained in cell F. The triangles (open and solid) are results from Eq. (3.1) using parameters given in Table VIII.

in Ref. 43). The parameters and t_m are given in Table IX. The solid lines in Fig. 10 represent such fits to the data at 6.85 and 28.00 bars of cell F. The minimum value t_m of t used in the fit is indicated by an arrow for each pressure. For $t > t_m$, deviations from the fits are less than 1% at all pressures. For $t < t_m$, the data show slight deviations from the extrapolation of the fit, although the general trend of the function and the data remain remarkably similar.

A deviation plot of data from the fit of Eq. (3.2) to the cell-F SVP results is given in Fig. 11. Here the solid circles are cell-F measurements made at SVP, and the solid triangles are the result of extrapolating cell-F isotherm data to SVP using Eq. (3.1) and Table VIII. Also shown as open inverted triangles are directly measured cell-H re-

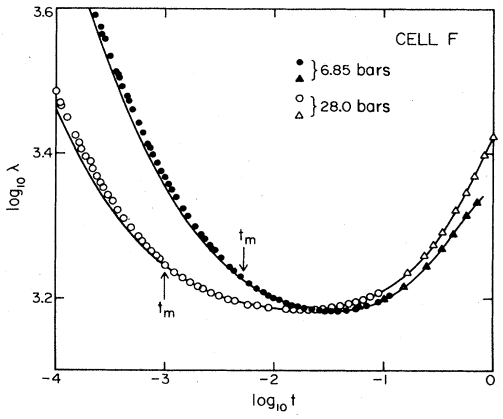

FIG. 10. Thermal conductivity λ at 6.85 bars (solid symbols) and 28.0 bars (open symbols) obtained in cell F over a limited range of t. The triangles (open and solid) are results from Eq. (3.1) using parameters given in Table VIII. The solid lines are fits given by Eq. (3.2) using parameters given in Table IX. The minimum t used in the fit for each pressure is indicated by t_m.

TABLE IX. Least-squares adjusted parameters of Eqs. (3.2a) and (3.2b) for cell F. The units of $\lambda_{\infty i}$ are in ergs s^{-1} cm^{-1} K^{-1}.

P (bars)	$10^3 t_m$	$\lambda_{\infty 0}$	$\lambda_{\infty 1}$	$\lambda_{\infty 2}$	$10^2\lambda_1$
SVP	7.0	1222	1574	−974	1.078
6.85	5.2	1390	1541	−693	0.562
14.73	2.8	1465	1585	−544	0.354
22.30	1.5	1480	1559	−417	0.243
28.00	1.0	1459	1533	−344	0.184

sults at SVP, but note that the spacing of cell H was adjusted so as to cause overall agreement with cell F. Clearly, all the data shown in Fig. 11 are consistent with each other.

In Fig. 12 we compare the measurements of cell E, of cell A (Ahlers and Behringer, $d=0.265$ cm),[14] of the result obtained by Dingus *et al.* ($d=0.147$ cm),[12] and of the data of Kerrisk and Keller[6,46] ($d=0.082$ cm) with the same fit to cell-F data that was used in Fig. 11. All data in this figure are absolute measurements, involving no adjustments or normalization. The overall agreement within a percent or so is therefore quite satisfying.

2. *Small t*

(a) Determination of $\hat{R}_\lambda$. For $t \lesssim 10^{-2}$ it is convenient to examine the effective amplitude $\hat{R}_\lambda$ of λ because this parameter varies only little with t and thus can be displayed graphically on a sensitive scale (it is also the parameter to be compared with theory in a subsequent paper).[11] We have[4]

$$\hat{R}_\lambda(t) \equiv (\lambda/k_B)/g_b(\xi C_p/k_B)^{1/2} , \tag{3.3}$$

where C_p is the heat capacity at constant pressure per unit volume, ξ is the correlation length, and

$$g_b = \sigma_\lambda k_B T_\lambda/\hbar . \tag{3.4}$$

Here $\sigma_\lambda = S_\lambda/R$ where $S_\lambda(P)$ is the entropy[17] at $T_\lambda(P)$ and $R=8.317$ J $mole^{-1}$ K^{-1} is the gas constant (i.e., g_b has the units of inverse time).

For the evaluation of $\hat{R}_\lambda$ from Eq. (3.3), we will ignore all regular dependences upon T that may enter g_b, as already implied by Eq. (3.4). We will therefore also restrict the use of $\hat{R}_\lambda$ to the range $t \lesssim 10^{-2}$, where the regular contributions presumably are only of order 1% or so. The necessary values of T_λ, σ_λ, and g_b have been collected in Table X for our isobars. The singular transients, which occur in C_p and ξ, will be included to lowest order in the evaluation of $\hat{R}_\lambda$, because they may be significant even for $t < 10^{-2}$. Thus, we write

$$C_p = A[(1/\alpha)(t^{-\alpha}-1)+\tilde{D}t^{\Delta-\alpha}+\tilde{B}] \tag{3.5}$$

and

$$\xi = \xi_0 t^{-\nu}(1+D_\xi t^\Delta) . \tag{3.6}$$

Under pressure, thermodynamic information about C_p is scarce. It exists primarily for[17] $t \lesssim 10^{-3}$ and for[47,48] $t \gtrsim 10^{-1}$ and is examined in detail in Appendix E. A function usable over the entire range $t < 1$ and suitable for interpolation between the two regions where data exist is provided by Eq. (3.5) with

$$A(T) = A_0(1+a_1 t+a_2 t^2) , \tag{3.7a}$$

$$\tilde{B}(T) = \tilde{B}_0(1+b_1 t+b_2 t^2) , \tag{3.7b}$$

and

$$\tilde{D}(T) = \tilde{D}_0(1+d_1 t) . \tag{3.7c}$$

In fitting the available data for pressures greater than SVP to Eqs. (3.5) and (3.7), we imposed the asymptotic behavior of C_p by fixing α, Δ, $\tilde{D}_0$, A_0, and $\tilde{B}_0$ at values obtained from an analysis of thermal-expansion-coefficient data at small t.[17] These fixed values are

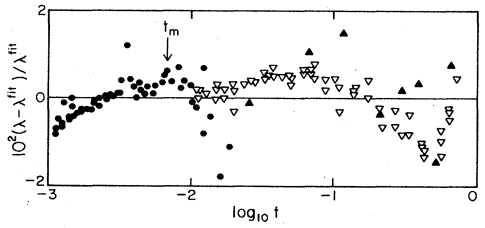

FIG. 11. Deviations of λ in percent at SVP of cell F (solid circles and triangles) and cell H (inverted open triangles) from Eq. (3.2) using parameters given in Table IX. t_m is the minimum value of t used in the fit as indicated by an arrow in the figure.

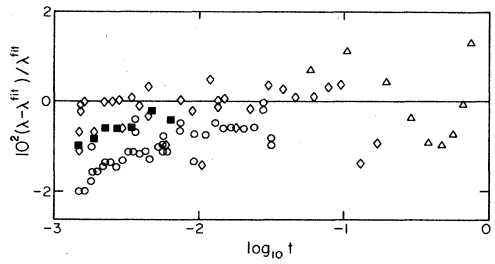

FIG. 12. Deviations of λ in percent at SVP of cell E (solid squares), cell A (Ref. 14, open circles), measurements from Ref. 12 (open lozenges), and Ref. 6 (open triangles) from Eq. (3.2).

TABLE X. Thermodynamic parameters for the isobars.

P (bars)	T_λ[a] (K)	σ_λ[b]	g_b (10^{11} s^{-1})
SVP	2.1720	0.7610	2.164
6.85	2.1010	0.6988	1.922
14.73	2.0020	0.6442	1.688
22.30	1.8929	0.5937	1.477
28.00	1.8006	0.5591	1.318

V_λ[a] (cm^3 mole^{-1})	$(\partial P/\partial T)_\lambda$[a] (bars K^{-1})	$(\partial S/\partial T)_\lambda$[b] (J mole^{-1} K^{-2})
27.38	−112.53	10.79
25.41	−86.17	5.47
23.99	−74.11	4.01
23.00	−65.09	3.44
22.39	−58.53	3.20

[a]Reference 34.
[b]Reference 17. We used $R=8.317$ J/mole K.

$$\alpha=-0.016\ , \tag{3.8}$$

$$\Delta=0.50\ , \tag{3.9}$$

$$\tilde{D}_0=1.352+0.0328P+0.0130P^2 \tag{3.10}$$

with P in bars and the values of A_0 and $\tilde{B}_0$ given in Table XI. The parameters a_i, b_i, and d_1 were least-squares adjusted so as to fit the large-t results as well. At SVP, where C_p data exist over a wide range of t,[19,47,48,49] we least-squares adjusted also A_0 and $\tilde{B}_0$, but we retained the constraints [Eqs. (3.8) to (3.10)]. The parameter values for our isobars are given in Table XI. Equations (3.5) and (3.7) with these coefficients will be useful also in the comparison of the data with the theory which is to be given elsewhere.[11] As examples we show in Fig. 13 the available data for C_p at SVP and 22.3 bars, together with the fit of Eqs. (3.5) and (3.7) to those data.

For the evaluation of the correlation length Eq. (3.6), we use

$$\nu=0.672\ , \tag{3.11}$$

Eq. (3.9) for Δ, and[50]

$$D_\xi=0.102\tilde{D}_0 \tag{3.12}$$

with $\tilde{D}_0$ given by Eq. (3.10). Values of ξ_0 can be estimated[51,17] and for our isobars are given in Table XI.

(b) Results. In Fig. 14 we show the values of $\hat{R}_\lambda$ derived from our cell-F data, using Eqs. (3.3) to (3.12) and Table XI, along three isobars. Numerical values for all five isobars are given in Tables V and VI.

In Fig. 15 we compare measurements at SVP for four different cells of reasonably large spacing. They are our cells E ($d=0.45$ cm) and F ($d=0.20$ cm), cell A of Ref. 14 ($d=0.26$ cm), and the data by Dingus *et al.*[12] ($d=0.15$ cm). Although there is excellent agreement for $t\gtrsim10^{-3}$ (see also Fig. 12), the various sets of data differ somewhat from each other at smaller t. Except for cell A, $\hat{R}_\lambda$ at constant $t<10^{-3}$ increases monotonically with decreasing d. As will be discussed in the next section, this trend can be removed to some extent by assuming a boundary resistance above T_λ which is substantially smaller than the extrapolation of Eq. (2.6) would suggest.

In Fig. 16 we show the results for cells F ($d=0.20$ cm), G ($d=0.10$ cm), and H ($d=0.013$ cm). For $t>10^{-3}$, where the data for cells G and H were normalized to those of cell F by adjusting d, the agreement is, of course, excellent. The monotonic trend of the data with d at constant $t\lesssim10^{-3}$ is similar to the trend observed in Fig. 15 for cells E, F, and the data of Dingus *et al.* The same trend exists also at higher pressures, as illustrated in Fig. 17 for cells E, F, and H at 22.3 bars.

(c) Effect of the boundary resistance. The boundary resistance of the various cells is not known with high accuracy for several reasons. First, the measurements in the superfluid phase (Sec. II E 5) involve large heat currents and small temperature differences, and therefore are not

TABLE XI. Parameters for C_p in Eqs. (3.5) and (3.7) and for ξ in Eq. (3.6).

P (bars)	A_0 (J mole^{-1} K^{-1})	a_1	a_2	$\tilde{B}_0$
SVP	6.156	−1.575	1.770	−1.826
6.85	5.806[a]	−1.697	0.884	−2.252[a]
14.73	5.791[a]	−1.779	0.920	−2.838[a]
22.30	5.937[a]	−1.482	0[a]	−3.346[a]
28.00	6.522[a]	0[a]	0[a]	−4.021[a]

b_1	b_2	$\tilde{D}_0$	d_1	$10^8\xi_0$ (cm)
−6.479	0[a]	0.356[a]	−6.148	1.432
−7.840	−15.85	2.188[a]	−17.92	1.425
−4.279	−11.88	4.656[a]	−7.368	1.399
2.561	0.634	9.556[a]	0.701	1.382
4.181	1.448	12.47[a]	1.228	1.314

[a]Parameter held constant in the fit.

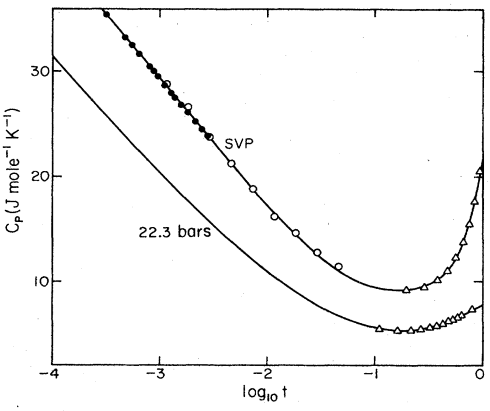

FIG. 13. Specific heat at constant pressure at SVP and 22.3 bars. The data are obtained from Ref. 19 (solid circles), Ref. 49 (open circles), and from Refs. 47 and 48 (open triangles). The solid lines are fits to the data at each pressure using Eqs. (3.5) and (3.7)—(3.10).

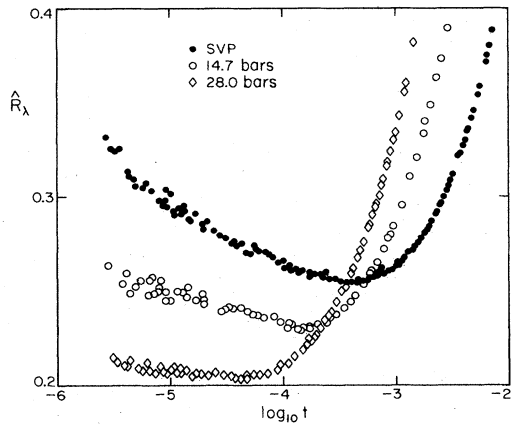

FIG. 14. The effective amplitude $\hat{R}_\lambda$ [Eq. (3.3)] of the thermal conductivity in cell F for different pressures as a function of the reduced temperature.

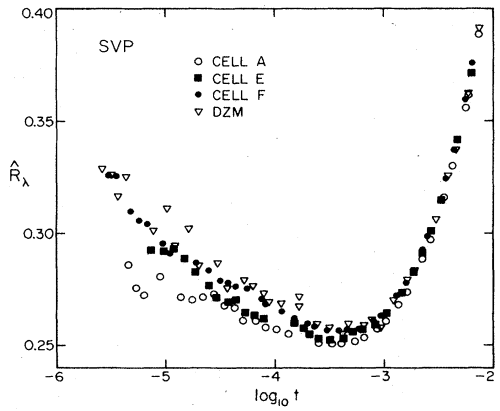

FIG. 15. The effective amplitude $\hat{R}_\lambda$ at SVP for λ obtained from cell A (Ref. 10), cell E, cell F, and from Ref. 12.

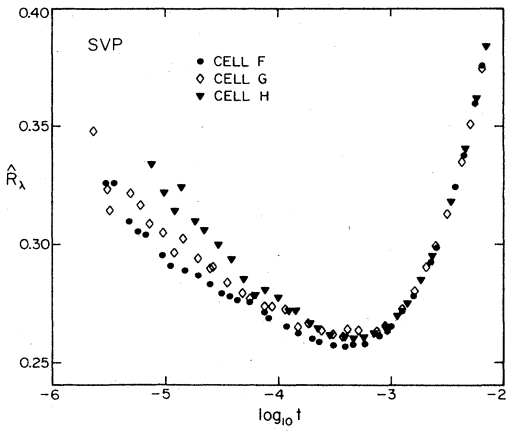

FIG. 16. The effective amplitude $\hat{R}_\lambda$ at SVP for cells F, G, and H using $f_b = 1$.

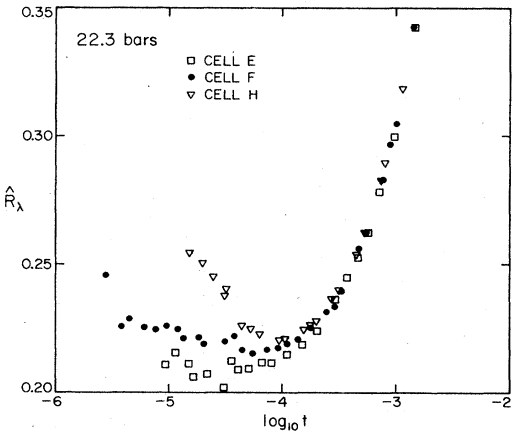

FIG. 17. The effective amplitude $\hat{R}_\lambda$ at 22.3 bars for cells E, F, and H using $f_b = 1$.

very precise. Second, for cells H and I the effective area is not well known because it is not clear whether the recess area [see Figs. 3(b) and 3(c)] should be included. We did not include it and thus may have systematically *under*estimated R_b for those cells by as much as 15%. Third, even though R_b does not show any singularity upon approaching T_λ from below [see Sec. II E 5 and Fig. 5(c)], it is by no means clear that a simple extrapolation to $T > T_\lambda$ of Eq. (2.6) for R_b is valid.[52]

It can be seen from Table III that it is not necessary to know R_b with high accuracy when the cell spacing is large. Thus, for cell F at SVP, the thermal conductivity given in Table VI for t near, say, 10^{-5} would be too low (high) by 0.7% if, in fact, R_b decreased (increased) by 50% upon crossing T_λ. At larger t the effect would be smaller. For the other cells the data in Table III should be changed in proportion to the inverse of the cell spacing to obtain estimates of the boundary-resistance contribution. Thus, for the shorter cells the effect of a change in R_b upon λ would be sizable. One therefore might expect

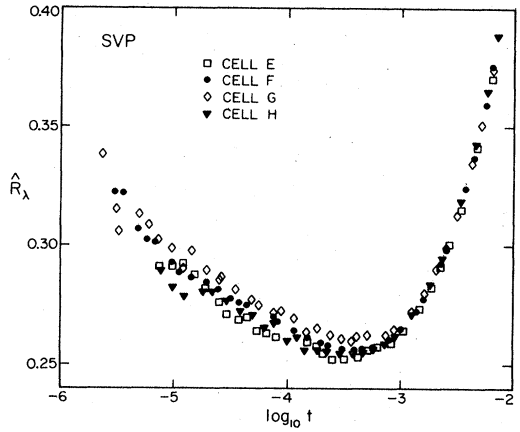

FIG. 18. The effective amplitude $\hat{R}_\lambda$ at SVP for cells E, F, G, and H using $f_b=0.57$.

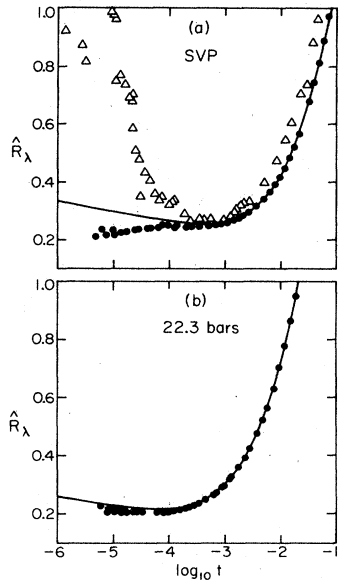

FIG. 20. The effective amplitude $\hat{R}_\lambda$ for cell I (solid circles) at SVP and 22.3 bars. The solid lines are a smooth representation of the cell-F results at the same pressures. In (a) the open triangles are results obtained from Refs. 7 and 8 with a cell spacing of 0.0033 cm.

that the trend with d of the results in Figs. 15 to 17 can largely be removed by assuming a drop in R_b at T_λ [note that the possible underestimate of R_b (the second point above) associated with the recess for cells H and I would be in the wrong direction]. We therefore defined a factor f_b by

$$\tilde{R}_b = f_b R_b \ , \tag{3.13}$$

where R_b is still given by Eq. (2.6). We used $\tilde{R}_b$ in the data analysis and computed new values of $\hat{R}_\lambda$ for $f_b \neq 1$. Figure 18 shows the results at SVP for cells E, F, G, and H which correspond to $f_b=0.57$. The trend of the data with d is removed, and systematic differences between the different cells are reduced. At 22.3 bars, the value $f_b=0.30$ results in Fig. 19, a dramatic improvement over Fig. 17.

We do not intend to suggest on the basis of the above analysis that the Kapitza resistance between liquid ^{4}He and our gold surfaces undergoes a discontinuous sizable drop upon crossing T_λ from below. Rather, our purpose is to demonstrate that the differences between data for the various cells are no larger than reasonable estimates of systematic uncertainties. These same reasonable estimates are quite small for cell F, corresponding at SVP to perhaps 1.2%, 0.7%, and 0.3% for $t=10^{-6}$, 10^{-5}, and 10^{-4}, respectively.

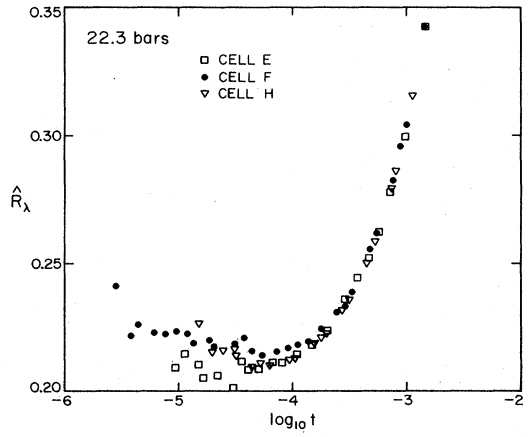

FIG. 19. The effective amplitude $\hat{R}_\lambda$ at 22.3 bars for cells E, F, and H using $f_b=0.30$.

(d) Ultrashort cells. In order to search for the size effect upon λ reported by Archibald *et al.*[7] and Weaver,[8] we made measurements in a cell with the very small spacing $d=0.0025$ cm (cell I). The results are not very accurate for two reasons. First, they are very sensitive to errors in boundary-resistance corrections [see Sec. III C 2(c) above]. Second, they had to be obtained with large heat currents which resulted in a less-stable thermal environment and required an extrapolation of the measurement of T_λ to zero current (see Sec. II E 2). Nonetheless, the results are in quite good agreement with the cell-F data. This is shown in Figs. 20(a) and 20(b). There, the cell-I data at SVP and 22.3 bars are given as solid circles, and the cell-F results are represented by the solid lines. Considering the possible systematic errors for the small d, the agreement is excellent.

At SVP our measurements in cell I can be compared with results by Archibald *et al.*,[7] as given by Weaver,[8] in a cell of similar spacing. The data[8] of Archibald *et al.* are given in Fig. 20(a) as open triangles. For small t, they lie significantly higher than our results. [Weaver,[8] when calculating λ from $\dot{Q}$ and ΔT, did not include any correction for R_b. If the effect of the boundary resistance were included in his data analysis, then the resulting conductivity would be even larger than shown in Fig. 20(a).] Clearly, our measurements do not confirm the size effect observed by Archibald *et al.*

IV. SUMMARY

We have presented measurements of the thermal conductivity λ of ^{4}He I along isotherms from 2.1 to 3.6 K and along isobars from SVP to 28.0 bars using cells with spacings ranging from 0.0025 to 0.453 cm. For the isotherms the pressure was varied from SVP to 30 bars, while isobar results covered the reduced temperature range $2\times10^{-6}\lesssim t\lesssim 0.1$.

We made careful corrections to the measurements for the heat conducted by the cell walls. These corrections were based on the numerical simulations of the appropriate two-dimensional heat-flow problem. The boundary resistance was measured for each cell in the superfluid phase, and we considered in detail the effect of its uncertainty on the thermal-conductivity results.

Our most accurate data were obtained in cell F which had a spacing of 0.20 cm. Larger spacings (cell E) led to excessively long thermal relaxation times, and therefore to larger random errors, and shorter spacings (cells H and I) required excessively large corrections for the boundary resistance. The cell-F data are tabulated in Table VI. Except for $t\lesssim 10^{-3}$ on isobars, they have an accuracy of 0.2% to 0.3%. For $t<10^{-3}$, the accuracy deteriorates gradually as t decreases, because of finite thermometer resolution and possible systematic errors associated with the boundary-resistance correction. At $t=10^{-4}$ and 10^{-5}, we estimate the uncertainty of the cell-F results to be about 0.6% and 1.0%, respectively.

In Table V we tabulate some data for cell E even though they are less precise then cell-F data. We do this because systematic errors due to errors in the spacing d are smallest for this cell.

Our measurements on isotherms agree well within error estimates with those of Kerrisk and Keller.[6] This was demonstrated in Figs. 8 and 12. At SVP our results also are consistent with those of Dingus *et al.*,[12] with those of Ahlers and Behringer (cell A),[14] and with those of Steinberg and Ahlers (cell G).[13] Our new results on isobars are systematically lower at small t than those of Ahlers[10] (cell D). We attribute the difference to problems in the early work with wall conduction and boundary-resistance corrections.

For the cells of small spacing d (cells G, H, and I), the absolute accuracy of the measurements was limited by the accuracy of the measurement of d. We therefore normalized those data for $t>10^{-2}$ to the absolute cell-F measurements. After that normalization, agreement with cell F was excellent over the entire range $10^{-3}\lesssim t\lesssim 1$, but for $t<10^{-3}$ the small-d results were systematically high. Agreement for small and large d could be achieved by assuming a boundary resistance R_b for He I considerably less than the value based on an extrapolation of the measurements of R_b in the He II region.

Finally, we made measurements in a cell of very small spacing ($d=0.0025$ cm, cell I). These measurements are not very accurate because the boundary-resistance correction is large, but they served to rule out a size effect upon λ of the magnitude proposed in previous work by others.[7,8]

From our most reliable measurements (cell F), we calculated the effective amplitude $\hat{R}_\lambda(t)$ of λ given by Eq. (3.3). This parameter will be needed in a subsequent paper[11] for the comparison[5] of our measurement with theoretical predictions.[1,3,4]

ACKNOWLEDGMENTS

We are grateful to V. Steinberg for permitting us to present and discuss the data obtained by Steinberg and Ahlers in cell G and to M. Dingus, F. Zhong, and H. Meyer for providing us with their data in numerical form. This work was supported by National Science Foundation Grants No. DMR-84-14804 and No. DMR-79-23289.

APPENDIX A: WALL CONDUCTION CORRECTIONS

In order to obtain quantitative results for the effective thermal length of the walls, we solved the appropriate two-dimensional heat-flow problem numerically, using an iterative method described, for instance, by Schenk or Ozisik.[53] The boundary conditions for this calculation are illustrated in Figs. 21(a) and 21(b). The shaded boundaries on the left-hand side of Figs. 21(a) and 21(b) and the right-hand side of Fig. 21(a) are adiabatic. The top and bottom of the cell are taken as isothermal since they are made of copper with a conductivity which is a factor of 10^3 to 10^4 higher than that of the fluid. The top of the cell is at $T=T_c=0$ and the bottom at $T=T_h=1$. The gap between the walls and the copper cylinders, filled either with epoxy [Fig. 21(a)] or helium [Fig. 21(b)], was taken to have a width of 0.0025 cm, but the results were not sensitive to this choice. For the thermal conductivity of the stainless-steel walls (λ_w), we used our measurements of the empty cell F. The thermal conductivity of ^{4}He I (λ) was also based on our cell-F measurements (these data are not very sensitive to small errors in the thermal length of the walls). The thermal conductivity of the epoxy was estimated from the data by Hartwig.[54] The temperature was evaluated at every point on a grid representing the cell cross section near the wall. Changing the grid size had virtually no effect upon the results. Figures 21(a) and 21(b) show the isotherms which were deduced by interpolation from our grid of temperature values.

Particularly for the small helium thickness d in Fig. 21(b), it is apparent that the vertical component of the temperature gradient can be much smaller in the wall than it is in the fluid. Therefore, the heat-conduction contribution of the walls would be significantly overestimated if it were based upon the thickness d of the cell and the conductivity λ_w of stainless steel. This effect decreases as λ diverges, and thus the effective thermal length (to be defined below) depends upon t.

On Fig. 21(a) the isotherms in the top half are a mirror image of those in the bottom. This symmetry does not exist for our short cells where liquid helium can penetrate the space between the top copper cylinder and the wall. In that case the isotherms depend upon t also because λ and thus the thermal attachment of the walls to the top

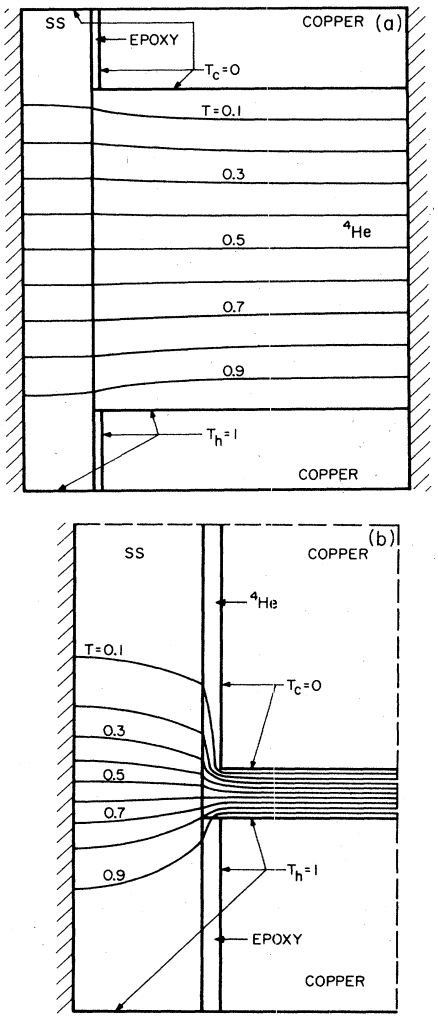

FIG. 21. (a) Isotherm plots obtained from a numerical simulation of the two-dimensional heat-flow problem for cell F at SVP and t=0.5. Only part of the cell is shown. The stainless-steel wall is indicated by SS. See text for discussions. (b) Isotherm plots obtained from a numerical simulation for cell H at SVP and t=0.5. Only part of the simulated section is shown.

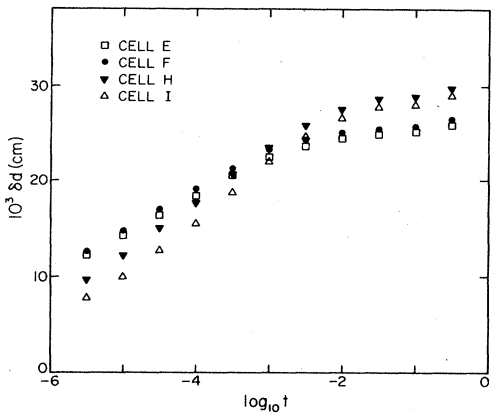

FIG. 22. The change of the effective thermal length obtained from numerical simulations at SVP for the walls of cells E, F, H, and I as a function of the reduced temperature.

copper cylinder depend upon t. This provides an additional reason for a change of the effective thermal length as t approaches zero and λ diverges.

The isotherms were used to calculate the total current $\dot{Q}$ passing through the midplane of the cell. The current $\dot{Q}_l$ passing through the liquid helium within the active area between the copper cylinders was calculated separately by assuming the ideal case without walls and epoxy and therefore with a uniform vertical temperature gradient. The difference $\dot{Q}_w=\dot{Q}-\dot{Q}_l$ was attributed to wall conduction and used to define an effective thermal length

$$d^{\text{eff}}=(\lambda_w A_w+\lambda A_{\text{gap}})\Delta T/\dot{Q}_w \ . \tag{A1}$$

Here $\Delta T=T_h-T_c=1$, A_w is the wall cross-sectional area and A_{gap} is the cross-sectional area of the epoxy- or helium-filled gap between the walls and the top or bottom copper cylinder.

Figure 22 shows results for $\delta d=d^{\text{eff}}-d$ as a function of $\log_{10}t$ for our four cells. One sees that δd changes by a factor of about 2 to 3 as t changes from 0.1 to 10^{-6}. It is only about 10% of d in the case of cells E or F, but for cell H it is of the same order as d, and for cell I it can be an order of magnitude larger than d. For this reason the wall contribution to the heat current is negligible for cell I but must be considered carefully for cells E, F, G, and H.

In order to find the appropriate thermal length of the empty cell F, calculations were performed in which the interior surfaces of the cell [see Fig. 21(a)] were adiabatic. We found δd=0.030 cm for all temperatures.

APPENDIX B: BOUNDARY RESISTANCE

As described in Sec. II C and shown in Figs. 3(a) and 3(b), the thermometers were immersed deep inside the copper cylinders which formed the cell ends and measured a temperature at a point physically close to the helium-copper interface. Figure 23 shows one-quarter of a cross section through a cell. The left boundary is the cell centerline and the right is at the circumference. The point labeled T_{th} shows the thermometer location. We carried out numerical heat-flow calculations for this geometry that were similar to those reported in Appendix A for the region near the cell walls. In the present case, however, the calculations had to be carried out in cylindrical coordinates.[53]

We represented the Kapitza resistance R_K by a thin fictitious layer of material of thickness d_K and conductivity λ_K such that

$$\lambda_K=d_K/R_K \ . \tag{B1}$$

The symmetry of the system guarantees that the horizontal midplane of the cell (lower edge of Fig. 23) is an isotherm; and thus we took its temperature to be constant in the calculation. All side walls (shaded in Fig. 23) were adiabatic. A uniform current left the system along the top copper surface.

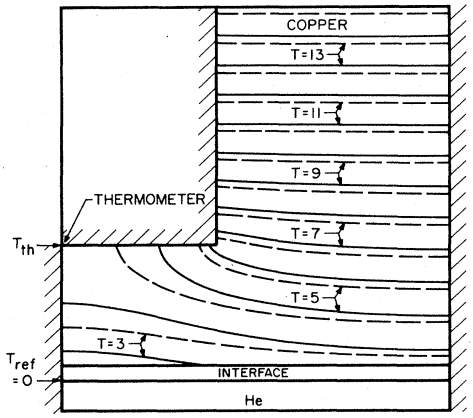

FIG. 23. Isotherms obtained from a numerical simulation of the two-dimensional heat-flow problem for cell F at SVP. The indicated temperatures are deviations from the temperature at the point indicated by T_{ref}. The dashed lines are isotherms obtained in the superfluid phase and the solid lines are isotherms obtained at $t=10^{-5}$ above T_λ. (See text for discussions.)

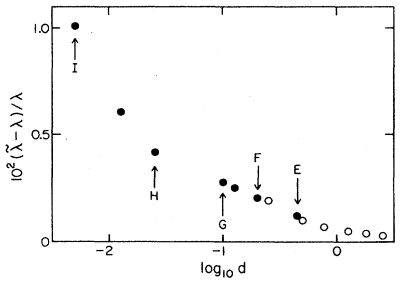

FIG. 24. Deviation of $\tilde{\lambda}$ [Eq. (B2) at SVP and $t=10^{-5}$] from the conductivity λ of the fluid. Different symbols correspond to different computational algorithms (see Ref. 43).

The thermal conductivity λ_{Cu} of copper was assumed to be 2 W/cm K for most of the calculations; but the effect of changing λ_{Cu} was explored also. In order to simulate the superfluid, we used a large value (e.g., 10^4 W/cm K) for the helium conductivity λ. For R_K we took as a starting value the measured boundary resistance R_b (about 1 K cm^2/W) reported in Sec. II E 5.

As a reference temperature, we used the temperature of the helium on the cell centerline at the top of the liquid layer, as shown in Fig. 23. In the superfluid, the temperature of the top of the liquid was virtually isothermal; but in the normal phase $\lambda \ll \lambda_{Cu}$ and horizontal gradients existed at the liquid top [but of course not at the midplane (bottom of Fig. 23)].

The calculation for He II yielded $\Delta T_b^{II}=T_{th}-T_{ref}$, as well as the contribution ΔT_{Cu}^{II} and $\Delta T_K^{II}=\Delta T_b^{II}-\Delta T_{Cu}^{II}$. The ratio $\Delta T_K^{II}/\Delta T_b^{II}$ was used to estimate a new value of R_K from the experimentally measured R_b. Iteration yielded a self-consistent value of R_K. At SVP we obtained $r=\Delta T_{Cu}^{II}/\Delta T_b^{II}=0.4$, indicating that the values of R_b reported in Fig. 5 should be multiplied roughly by 0.6 to give R_K. However, this factor is sensitive to λ_{Cu} which is not known well (for $\lambda_{Cu}=4$ W/cm K, for example, we obtained $r=0.2$).

For $T>T_\lambda$, we carried out the same calculation, using the R_K determined below T_λ and the appropriate λ for the fluid. Thus, we assumed R_K is continuous and slowly varying near T_λ. Figure 23 shows isotherms (in arbitrary units) in the copper obtained for a helium layer thickness $d=0.20$ cm, $t=10^{-5}$, and SVP ($\lambda=0.0018$ W/cm K) as solid lines (for clarify no isotherms are shown in the helium and Kapitza layers). The dashed lines are the corresponding isotherms obtained for $T<T_\lambda$ ($\lambda=10^4$ W/cm K). It is apparent that $\Delta T_b^I>\Delta T_b^{II}$, even though the same value of R_b was used on both sides of T_λ. This effect results from the change in the horizontal gradients in the liquid when the phase transition is crossed. The ratio $\Delta T_b^I/\Delta T_b^{II}$ was found to be 1.16 for the particular example of Fig. 23, and increased smoothly with the thickness of the helium layer. Thus, the *effective* boundary resistance above T_λ will be larger than the measured R_b below T_λ.

The numerical results for the total temperature differences across the copper, the Kapitza layer, and the helium ΔT^I and ΔT^{II} for the two phases can be used to estimate the "experimental" value of λ, namely

$$\tilde{\lambda}=(\dot{Q}_l/A)d/(\Delta T^I-\Delta T_b^{II}) . \quad \text{(B2)}$$

A comparison with the value of λ used in the calculation yields the error $(\tilde{\lambda}-\lambda)/\lambda$. This error is shown in Fig. 24 as a function of the cell thickness d for $t=10^{-5}$ and SVP. The two different symbols correspond to different computational algorithms.[43] For our larger cells (E and F) the error due to this effect is only about 0.2% and has been neglected. For the shortest cell the effect becomes as large as 1%.

Table XII gives a few results of $(\tilde{\lambda}-\lambda)/\lambda$ for cell F at various pressures and temperatures. The effect is in the right direction to explain the difference in the conductivity of cells F and H; but the magnitude is much too small. Thus, to explain that difference one still needs to invoke a genuine drop of R_K at or very near the phase transition.

APPENDIX C: CURVATURE CORRECTION

We define the experimental conductivity $\bar{\lambda}(t,\Delta T)$ by Eqs. (2.7) and (2.8) in terms of finite temperature differences ΔT produces by finite currents $\dot{Q}_l/A$ and assigned $\bar{\lambda}$ to a reduced temperature $t=(T_c+\Delta T/2)/T_\lambda-1$ [Eq.

TABLE XII. Error in λ due to horizontal thermal gradients in the copper cylinders comprising the cell ends (for details, see text of Appendix B). We used $\lambda_{Cu}=2$ W/cm K, and $\Delta T_K^{II}/\Delta T_b^{II}=0.57$ and 0.78 at SVP and 28 bars, respectively.

P		$\frac{(\tilde{\lambda}-\lambda)}{\lambda}$	
(bars)	t	Cell F	Cell H
SVP	10^{-6}	0.0030	
SVP	10^{-5}	0.0020	0.0042
SVP	10^{-4}	0.0011	
SVP	10^{-3}	0.0005	
28.0	10^{-5}	0.0011	

(2.9)]. This procedure yields the actual conductivity λ only if λ is either constant or a linear function of T. If λ depends upon T in a nonlinear manner, a "curvature correction" is required. We find the correction factor by using an approximate representation of λ by a fit of the empirical function

$$\lambda = at^{-x}(1+bt^y) \tag{C1}$$

to $\bar{\lambda}$ and by assuming that locally λ has its zero-power value. Thus, Eq. (C1) can be used to integrate the relation

$$(\dot{Q}_l/A)dz = -\lambda\, dT \tag{C2}$$

from $z=0$ (cell bottom) to $z=d$ (cell top), and from

$$t_2 = (T_h - T_\lambda)/T_\lambda \tag{C3a}$$

to

$$t_1 = (T_c - T_\lambda)/T_\lambda \tag{C3b}$$

to give

$$\dot{Q}_l/A = -(a\lambda/d)D\ , \tag{C4a}$$

where

$$D = (t_1^{z_1} - t_2^{z_1})/z_1 + b(t_1^{z_2} - t_2^{z_2})/z_2 \tag{C4b}$$

with

$$z_1 = 1-x,\ \ z_2 = 1-x+y\ . \tag{C5}$$

The average conductivity $\bar{\lambda} = -aD/(t_2 - t_1)$ is to be compared with the conductivity λ given by Eq. (C1) for $t = t_1 + \Delta T/2T_\lambda$. For

$$f_{\text{curv}} \equiv \lambda(t)/\bar{\lambda}(t,\Delta T) \tag{C6}$$

one finds

$$f_{\text{curv}} = t^{-x}(1+bt^y)(t_1 - t_2)/D \tag{C7}$$

with D given by Eq. (C4b). Equations (C6) and (C7) with the measured $\bar{\lambda}$ yield $\lambda(t)$.

The fit of Eq. (C1) to the data can be iterated starting with the estimate $\bar{\lambda} = \lambda$. In practice, the initial fit to $\bar{\lambda}$ yielded f_{curv} with adequate accuracy.

The maximum value of f_{curv} is equal to unity. The minimum value is obtained when $t_1 = 0$, i.e., the cold end of the sample is at T_λ. For all of our data points, f_{curv} was larger than 0.8, and, for most of them, it exceeded 0.98.

An accurate treatment of the curvature correction was particularly important for the study of the power dependence of λ. The data with the largest power in Figs. 6(a) and 6(b) had t_1 nearly equal to zero and thus required a relatively large curvature correction (small f_{curv}).

TABLE XIII. Effective cell spacing obtained by comparing the conductivity of each cell with cell F for $t \gtrsim 10^{-2}$. We used $f_B = 1$, i.e., R_b as given by Eq. (2.6).

P (bars)	Cell spacing (cm) G	H	I
SVP	0.1033	0.012 90	0.002 621
6.85		0.013 01	
14.73		0.013 12	
22.30		0.013 24	0.003 238
28.00		0.013 32	

TABLE XIV. Effective cell spacing d and boundary-resistance factor f_b of cell H obtained by comparing the conductivity with that of cell F. The value of R_b given by Eq. (2.6) was reduced by a factor f_b [Eq. (3.13)], and f_b as well as d were least-squares adjusted to the cell-F results for $t \gtrsim 10^{-2}$.

P (bars)	f_b	Spacing d (cm)
SVP	0.570	0.012 97
6.85	0.367	0.013 14
14.73	0.365	0.013 27
22.30	0.299	0.013 44
28.00	0.154	0.013 59

APPENDIX D: CELL SPACINGS OF THE SHORT CELLS

For the shorter cells G, H, and I, the relative error of the direct measurement of the cell spacing d is larger than other errors of the conductivity measurements. Thus, for these cells the conductivity measurements were normalized to those of cell F over the range $0.01 \lesssim t \lesssim 0.5$ by a least-squares procedure. This was done separately on each isobar and yielded the values of d given in Table XIII. For cell H where data exist on all isobars, the spacing increases linearly with P. We attribute the change in d with P to the elastic elongation of the cell walls of cells H and I. For these cells the free length includes the distance along the top cylinder up to the top of the recess [see Figs. 3(b) and 3(c)] and is equal to $d + 0.25$ cm. The relative change of this length with P, as reflected in the cell-H spacings given in Table XIII, is consistent with Young's modulus of stainless steel at low temperature.[55] For cells E and F where the free length of the walls was equal to d [see Fig. 3(a)], the elongation was estimated on the basis of the cell-H data or Young's modulus[55] to be less than 0.1% of d and thus negligible.

As discussed in Sec. III C 2(c), changing the boundary resistance R_b significantly affects the results for λ close to T_λ for the short cells. However, changing R_b also changes the normalization and the results for d, albeit only slightly. We therefore used the results for d in Table XIII as a starting point and adjusted f_b in the calculation

TABLE XV. Parameters for C_p as given by Eq. (E1) derived from thermal-expansion-coefficient measurements (Refs. 15 and 17) in the range $t \lesssim 10^{-3}$. We used $\Delta = 0.5$ and $\alpha = -0.016$.

P (bars)	A_0 (J mole^{-1} K^{-1})	B_0 (J mole^{-1} K^{-1})	D_0
6.85	5.806	349.8	−0.035
14.73	5.791	345.5	−0.075
22.30	5.937	351.2	−0.137
28.00	6.522	381.4	−0.200

TABLE XVI. C_v (interpolated from Ref. 48) and C_p data at high temperatures in units of J mole^{-1} K^{-1}.

	P (bars)							
	6.85		14.73		22.30		28.00	
T (K)	C_v	C_p	C_v	C_p	C_v	C_p	C_v	C_p
1.9							5.37	5.38
2.0					5.77	5.79	4.81	4.88
2.1			7.52	7.54	5.40	5.50	4.70	4.83
2.2	9.18	9.25	6.37	6.47	5.21	5.34	4.70	4.88
2.3	7.68	7.86	6.02	6.20	5.20	5.38	4.77	5.00
2.4	7.13	7.43	5.92	6.17	5.26	5.51	4.50	5.17
2.5	6.94	7.37	5.92	6.25	5.35	5.64	5.02	5.34
2.6	6.92	7.46	5.99	6.40	5.46	5.81	5.15	5.52
2.7	6.93	7.56	6.08	6.56	5.59	5.98	5.30	5.72
2.8	6.97	7.70	6.18	6.74	5.73	6.19	5.47	5.96
2.9	7.03	7.92	6.92	6.29	5.88	6.40	5.64	6.19
3.0	7.10	8.12	6.40	7.10	6.02	6.60	5.80	6.39

of λ for cell F and cell H so as to fit the short-cell data to cell F on a given isobar over the range $10^{-6} \lesssim t \lesssim 10^{-4}$. The procedure was carried out iteratively by recalculating λ with the new f_b in the range $10^{-2} \leq t \leq 0.5$ and obtaining new values of d. Table XIV shows the converged results for cell H. The pressure dependence of d is not changed very much. The values of f_b decrease approximately linearly with P.

A similar analysis using cells F and G at SVP yielded $f_b = 0.56$, consistent with the cells F and H comparison. The cell G spacing with $f_b = 0.56$ was 0.1034 cm.

The spacings for cells H and I determined by this comparison at SVP with cell F were well within the uncertainty of the original direct measurement of d. For cell G the direct measurement is slightly smaller (see Table I). We adopted the spacings in Tables XII and XIII for the analysis of the data for cells G, H, and I.

APPENDIX E: HEAT CAPACITY AT CONSTANT PRESSURE

Thermodynamic properties near T_λ were reviewed and analyzed recently by Singsaas and Ahlers.[17] At SVP there are direct heat-capacity measurements[19,47,49] over a wide range of t. At the higher temperatures where the measurements differ significantly from C_p, values of C_p have been obtained from the data with the help of additional thermodynamic information.[5]

At elevated pressures, experimental thermodynamic data are more scarce. Near $T_\lambda(P)$, the most reliable[17] measurements are those of the isobaric thermal expansion coefficient β_p.[15] Those data were reanalyzed[17] and used to find the parameters A_0, B_0, and D_0 in the power law

$$C_p = (A_0/\alpha)t^{-\alpha}(1+D_0 t^{\Delta}) + B_0 \tag{E1}$$

as a function of P. The values interpolated to our isobars are given in Table XV. We will use Eq. (E1) with those parameters to represent C_p at small t.

For P greater than SVP and larger t, the only measurements we know of are those by Lounasmaa and Kojo[48] of C_v. We interpolated between those data to obtain C_v on our isobars at intervals of 0.1 K. Those results are shown in Table XVI. They were used to derive the C_p values in Table XVI from the thermodynamic relation

$$C_p = C_v + \beta_P^2 VT/\kappa_T \ , \tag{E2}$$

where κ_T is the isothermal compressibility. Values of V, β_P, and κ_T were obtained from the measurements of Elwell and Meyer.[56]

The estimates of C_p obtained in the above manner primarily are for the range $t \gtrsim 0.1$, thus leaving a gap with no data for $3\times10^{-3} \lesssim t \lesssim 0.1$. In order to span that gap, we fitted the data in Table XVI to Eqs. (3.5) and (3.7) using the parameters in Table XV and the relations

$$\tilde{D}_0 = D_0, \quad \tilde{B}_0 = B_0/A_0 + 1/\alpha \tag{E3}$$

to fix A_0, $\tilde{B}_0$, and $\tilde{D}_0$. The remaining parameters a_i, b_i, and d_1 in Eq. (3.7) were least-squares adjusted to achieve a fit to the high-temperature data in Table XVI. At SVP we carried out a fit of the same Eqs. (3.5) and (3.7) to the existing data, but since there are C_p data over a wide range of t, we least-squares adjusted also the parameters A_0 and $\tilde{B}_0$ [the value of $\tilde{D}_0$ was fixed at that given by Eq. (3.10)]. All the parameters for Eqs. (3.5) and (3.7) are collected in Table XI. The fits were compared with the experimental data for C_p in Fig. 13. Where data exist, the agreement is good. We believe that Eqs. (3.5) and (3.7) yield C_p at all $t \lesssim 1$ to within a few percent.

[1]A number of reviews describe this in detail. Among them are V. Dohm and R. Folk, in *Advances in Solid State Physics,* edited by P. Grosse (Vieweg, Braunschweig, 1982), Vol. 22; V. Dohm and R. Folk, Physica **109&110B**, 1549 (1982); P. C. Hohenberg, *ibid.* **109&110B**, 1436 (1982); G. Ahlers, in *Phase Transitions,* edited by M. Levy, J. C. Le Guillou, and J. Zinn-Justin (Plenum, New York, 1980), p. 1; G. Ahlers, Rev. Mod. Phys. **52**, 489 (1980). A recent extensive experimental investigation and the comparison of its results with the theory are reported by R. Mehrotra and G. Ahlers, Phys. Rev. B **30**, 5116 (1984).

[2]See, for instance, G. Ahlers in Ref. 1.

[3]C. De Dominicis and L. Peliti, Phys. Rev. Lett. **38**, 505 (1977); Phys. Rev. B **18**, 353 (1978); V. Dohm, Z. Phys. B **31**, 327 (1978); V. Dohm, Z. Phys. (to be published); and private communication.

[4]B. I. Halperin, P. C. Hohenberg, and E. D. Siggia, Phys. Rev. Lett. **32**, 1289 (1974); Phys. Rev. B **13**, 1299 (1976); P. C. Hohenberg and B. I. Halperin, Rev. Mod. Phys. **49**, 435 (1977).

[5]G. Ahlers, P. C. Hohenberg, and A. Kornblit, Phys. Rev. Lett. **36**, 493 (1981); Phys. Rev. B **25**, 3136 (1982).

[6]J. Kerrisk and W. E. Keller, Bull. Am. Phys. Soc. **12**, 550 (1967); Phys. Rev. **177**, 341 (1969); J. Kerrisk, Ph.D. thesis, The University of New Mexico, 1968.

[7]M. Archibald, J. M. Mochel, and L. Weaver, Phys. Rev. Lett. **21**, 1156 (1968); in *Proceedings of the Eleventh International Conference on Low Temperature Physics,* edited by J. F. Allen, D. M. Finlayson, and D. M. McCall (University of St. Andrews, St. Andrews, Scotland, 1968), p. 211.

[8]L. Weaver, Ph.D. thesis, The University of Illinois, 1970.

[9]G. Ahlers, Phys. Rev. Lett. **21**, 1159 (1969); in *Proceedings of the Eleventh International Conference on Low Temperature Physics,* edited by J. F. Allen, D. M. Finlayson, and D. M. McCall (University of St. Andrews, St. Andrews, Scotland, 1968), p. 203.

[10]G. Ahlers, in *Proceedings of the Twelfth International Conference on Low Tmeperature Physics,* edited by E. Kanda (Academic, Tokyo, 1971), p. 21.

[11]W. Y. Tam and G. Ahlers, Phys. Rev. B (to be published).

[12]M. Dingus, F. Zhong, and H. Meyer (unpublished); see, also, D. Gestrich, M. Dingus, and H. Meyer, Phys. Lett. **99A**, 331 (1983).

[13]V. Steinberg and G. Ahlers (unpublished).

[14]G. Ahlers and R. P. Behringer, as reported by Ahlers *et al.*, Ref. 5.

[15]K. H. Mueller, G. Ahlers, and F. Pobell, Phys. Rev. B **14**, 2096 (1976).

[16]V. Steinberg and G. Ahlers, J. Low Temp. Phys. **53**, 255 (1983).

[17]A. Singsaas and G. Ahlers, Phys. Rev. B **29**, 4951 (1984); **30**, 5103 (1984).

[18]L. D. DeLong, O. G. Symko, and J. C. Wheatley, Rev. Sci. Instrum. **42**, 147 (1971).

[19]G. Ahlers, Phys. Rev. A **3**, 696 (1971).

[20]P. R. Roach, J. B. Ketterson, and M. Kuchnir, Rev. Sci. Instrum. **43**, 898 (1972).

[21]H. Van Dijk, M. Durieux, J. R. Clement, and J. K. Logan, Nat. Bur. Stand. (U.S.), Monogr. No. 10 (U.S. GPO, Washington, D.C., 1960).

[22]G. C. Straty and E. D. Adams, Rev. Sci. Instrum. **40**, 1939 (1969).

[23]Singer, ac Ratio Standard, model No. 1011.

[24]Princeton Applied Research, model No. 124A with model No. 185 preamplifier.

[25]M. Chan, M. Ryschleewitsch, and H. Meyer, J. Low Temp. Phys. **26**, 213 (1977).

[26]Texas Instruments, Inc., Precision Pressure Gauge, model No. 145-02.

[27]MKS Instruments, Inc., type BHS-10000 Baratron Pressure Gauge.

[28]D. S. Greywall and P. A. Busch, Rev. Sci. Instrum. **51**, 509 (1980).

[29]The plating was done using the gold-plating solution, Atomex, by Engelhard Industries West, Inc.

[30]R. P. Behringer and G. Ahlers, J. Fluid Mech. **125**, 219 (1982).

[31]Allen-Bradley 0.1-W, 34-Ω carbon resistors.

[32]Cryocal, model No. CR1000 ^{3}He.

[33]General Resistance, 5 kΩ (±0.01%).

[34]H. A. Kierstead, Phys. Rev. **162**, 153 (1967).

[35]Linear Research, San Diego, CA, model No. LR-130 temperature controller.

[36]G. L. Pollack, Rev. Mod. Phys. **41**, 48 (1969).

[37]See, for instance, G. Ahlers, Phys. Rev. Lett. **22**, 54 (1969).

[38]See, for instance, H. J. Mikeska, Phys. Rev. **179**, 166 (1969); or A. Onuki, Prog. Theor. Phys. **70**, 875 (1983).

[39]V. J. Johnsson, Wright Air Development Division Technical Report 60-65, 1960, Part II; J. F. Kerrisk, in Ref. 6.

[40]P. L. Kapitza, J. Phys. (Moscow) **4**, 181 (1941).

[41]R. C. Johnson and W. A. Little, Phys. Rev. **130**, 596 (1963).

[42]L. S. Challis, K. Dransfeld, and J. Wilks, Proc. R. Soc. London, Series A **260**, 31 (1960); Wey-Yen Kuang, Zh. Eksp. Teor. Fiz. **42**, 921 (1962) [Sov. Phys.—JETP **15**, 635 (1962)]; A. C. Anderson, J. I. Connolly, and J. C. Wheatley, Phys. Rev. A **910**, 135 (1964); S. W. VanSciver, Cryogenics **18**, 521 (1978).

[43]W. Y. Tam, Ph.D. thesis, University of California, Santa Barbara, CA, 1985.

[44]See AIP document No. PAPS-PRBMD-32-5932-62 for 62 pages of tabulated data. Order by PAPS number and journal reference from American Institute of Physics, Physics Auxiliary Publication Service, 335 East 45th St., New York, NY 10017. The price is $1.50 for a microfiche (98 pages) or $5.00 for photocopies of up to 30 pages, and $0.15 for each additional page over 30 pages. Airmail additional. Make checks payable to the American Institute of Physics.

[45]R. A. Ferrell and J. K. Bhattacharjee, Phys. Rev. Lett. **42**, 1638 (1979).

[46]We use the extrapolations of the data by Kerrisk (Ref. 6) to SVP which were tabulated in Ref. 5.

[47]R. W. Hill and O. V. Lounasmaa, Philos. Mag. **2**, 143 (1957).

[48]O. V. Lounasmaa and E. Kojo, Physica **VI**, 36 (1959).

[49]M. J. Buckingham and W. M. Fairbank, in *Progress in Low Temperature Physics,* edited by C. J. Gorter (North-Holland, Amsterdam, 1969), Vol. III, p. 80.

[50]C. Bagnuls and C. Bervillier, Phys. Rev. B **24**, 1226 (1981).

[51]P. C. Hohenberg, A. Aharony, B. I. Halperin, and E. D. Siggia, Phys. Rev. B **13**, 2986 (1976).

[52]For instance, the thermal conductivity in ^{3}He-^{4}He mixtures reveals no evidence of a singularity when T_λ is approached from below. Nonetheless, upon crossing T_λ, it decreases rapidly and has a singular dependence upon t. See, for instance, G. Ahlers, Phys. Rev. Lett. **24**, 1333 (1970).

[53]H. Schenk, Jr., *Fortran Methods in Heat Flow* (The Ronald Press Co., New York, 1963); M. Necati Ozisik, *Boundary Value Problems of Heat Conduction* (International Textbook, Scranton, PA, 1968).

[54]G. Hartwig, Adv. Cryog. Eng. **24**, 171 (1977).
[55]H. M. Ledbetter, in *Proceedings of the Second International Cryogenics Materials Conference,* edited by K. D. Timmerhaus, R. D. Reed, and A. T. Clark (Plenum, New York, 1978), p. 103.
[56]D. L. Elwell and H. Meyer, Phys. Rev. **164**, 245 (1967).